**TECHNICAL REPORT** **Report No: ESSO-INCOIS-OMARS-TR-01(2025)**

# Evaluation of NCMRWF analysis fields using observational, reanalysis, and satellite observations.

By

Srinivasu Kotta, Hasibur Rahaman, Anuradha Modi, Kameshwari Nunna, Hari Kumar R, Raheema Rahman, Sudheer Joseph, Balakrishnan Nair T.M

Indian National Centre for Ocean Information Services (INCOIS),
Earth System Science Organization (ESSO),
Ministry of Earth Sciences (MoES),
Hyderabad,
India

www.incois.gov.in

**DOCUMENT CONTROL SHEET**
**Earth System Science Organization (ESSO)**
**Ministry of Earth Sciences (MoES)**
**Indian National Centre for Ocean Information Services (INCOIS)**

**ESSO Document Number:** ESSO-INCOIS-OMARS-TR-01(2025)
**Title of the report:** Evaluation of NCMRWF analysis fields using observational, reanalysis, and satellite observations.

**Author(s):**
[Srinivasu Kotta, Hasibur Rahaman, Anuradha Modi, Kameshwari Nunna, Hari Kumar R, Sudheer Joseph, Balakrishnan Nair T.M]

**Originating unit:** OMARS
**Type of Document:** Technical Report (TR)
**Number of pages:** 47
**Number of figures:** 36
**Number of references:** 22
**Keywords**: NCMRWF Analysis fields, Winds, Air temperature, humidity
**Security classification:** Open
**Distribution:** Open
**Date of publication:**
**Abstract:**

The Indian summer monsoon is crucial for the country in various aspects, including agriculture, water resources, and economic stability. Hence, reliable monsoon forecasts are essential. INCOIS provides near real-time global analysis with the Global Ocean Data Assimilation System (GODAS), which was adopted from NOAA/NCEP in 2013. This analysis is used for the crucial initial conditions for the CFSv2 coupled model, which was used for the seasonal Indian Summer Monsoon Rainfall forecast. Accurate ocean initialization is required for better ISMR seasonal prediction. GODAS analysis was produced using the forcing fields from NCMRWF GFS atmospheric analysis. Bulk-algorithm is used to compute turbulent heat and momentum fluxes using the near-surface NCMRWF analysis fields. Studies show that errors in the input fields, particularly near-surface wind, air temperature (AT), and humidity, significantly affect the heat and momentum flux computation using a bulk algorithm. In this study, we evaluate near-surface wind, air temperature, and humidity from NCMRWF analysis with RAMA buoy observations. We further used NCMRWF reanalysis, ERA5 reanalysis, and satellite-derived CCMP wind products to quantify the spatial distribution of these fields as well. For AT and relative humidity (RH) we used OAFlux. The evaluation study shows that NCMRWF analysis products outperformed the other products when compared with buoy observations. Among the NCMRWF and ERA5 reanalysis products, NCMRWF outperformed. ERA5 wind and AT underestimate the other products as well as buoy observations. For AT and RH, the RMSE, CC, and bias for all the products are the least in NCMRWF analysis, then NCMRWF reanalysis, OAFlux, and ERA5, respectively. CCMP wind performance is poorest in the wind field among all the products used in this study.

| | Content | Pg.No |
|---|---|---|

**Evaluation of NCMRWF analysis fields using observational, reanalysis, and satellite observations**

Srinivasu Kotta, Hasibur Rahaman, Anuradha Modi, Kameshwari Nunna, Hari Kumar R, Sudheer Joseph, Balakrishnan Nair T.M

**Abstract:**

The Indian summer monsoon is crucial for the country in various aspects, including agriculture, water resources, and economic stability. Hence, reliable monsoon forecasts are essential. INCOIS provides near real-time global analysis with the Global Ocean Data Assimilation System (GODAS), which was adopted from NOAA/NCEP in 2013. This analysis is used for the crucial initial conditions for the CFSv2 coupled model, which was used for the seasonal Indian Summer Monsoon Rainfall forecast. Accurate ocean initialization is required for better ISMR seasonal prediction. GODAS analysis was produced using the forcing fields from NCMRWF GFS atmospheric analysis. Bulk-algorithm is used to compute turbulent heat and momentum fluxes using the near-surface NCMRWF analysis fields. Studies show that errors in the input fields, particularly near-surface wind, air temperature, and humidity, significantly affect the heat and momentum flux computation using a bulk algorithm. In this study, we evaluate near-surface wind, air temperature, and humidity from NCMRWF analysis with RAMA buoy observations. We further used NCMRWF reanalysis, ERA5 reanalysis, and satellite-derived CCMP wind products to quantify the spatial distribution of these fields as well. For air temperature (AT) and relative humidity (RH) we used OAFlux. The evaluation study shows that NCMRWF analysis products outperformed the other products when compared with buoy observations. Among the NCMRWF and ERA5 reanalysis products, NCMRWF outperformed. ERA5 wind and air temperature underestimate the other products as well as buoy observations. For AT and RH, the RMSE, CC, and bias for all the products are the least in NCMRWF analysis, then NCMRWF reanalysis, OAFlux, and ERA5, respectively. CCMP wind performance is poorest in the wind field among all the products used in this study.

## 1. Introduction:

Models are invaluable tools for understanding the ocean-atmosphere system, its interactions, and future climate scenarios, as well as for short-term forecasts of phenomena like cyclones, ocean states, and heatwaves. Depending on the objectives, various types of models are utilized. Ocean General Circulation Models (GCMs), such as Princeton Ocean Models (POMs), Regional Ocean Models (ROMs), Modular Ocean Models (MOMs), Hybrid Coordinate Ocean Models (HYCOMs), and others, were used by different operational, research organizations ,and academia to comprehend ocean processes and anticipate future ocean states. These models differ primarily in parametrization schemes, grid types, and other characteristics. Besides methodology, the quality of input data, including surface boundary forcing fields, significantly influences ocean model simulations (Goswami and Rajgopal 2003). Surface heat and momentum fluxes are pivotal parameters in the surface boundary conditions of ocean models, with wind speed, air temperature, and humidity crucial for estimating turbulent heat fluxes. These fluxes are integral to air-sea interaction processes at the ocean-atmosphere interface, driving ocean models.

The primary sources of atmospheric and ocean surface observations integrated with model output for analysis data include remote sensing data, ship measurements, buoy observations, radiosonde data, pilot balloon data, and outputs from numerical models. These diverse sources of observational data are assimilated into model simulations to enhance the accuracy and reliability of the analysis data, providing valuable insights into weather and oceanic conditions. Since 1994, the NCMRWF has been providing atmospheric analysis products to leading operational centers in India, such as INCOIS and IMD. Initially, NCMRWF utilized the National Center for Environmental Prediction (NCEP) Global Forecast System (GFS) for analysis and forecasting. In 2012, NCMRWF started the NCMRWF Unified Model (NCUM) with the support of UK Met Office. The GFS and NCUM systems have undergone multiple upgrades over the years to incorporate advancements in science and technology (Prasad et al., 2016, Sumit et.al., 2016). Ensuring the quality of model analyses is pivotal, as they are used for numerous applications, including serving as external atmospheric forcing in ocean or sea ice models.

Previous studies, such as those by Goswami and Rajgopal (2003), evaluated the NCMRWF analysis winds with reference to the QuickSCAT satellite winds over the Indian Ocean. They observed a high bias over the equatorial region and noted improvements in wind accuracy after the simulation of precipitation by the forecast model. Similarly, Sanjib et al. (2009) evaluated the ECMWF and NCEP winds using QuickSCAT level 2 and level 3 winds. They reported that ECMWF and NCEP analysis winds exhibited biases over the

regions from 10°S to 20°S and 5°S to 20°S, respectively. Prediction of the future state of the atmosphere/ocean by models highly depends on the initial and boundary conditions (analysis data) used by the model. Hence, the validation of analysis data is crucial for model performance, as it helps identify errors and biases. By validating the data, valuable feedback can be obtained to improve model accuracy and reliability, which is essential for producing accurate weather forecasts and analyses.

The Indian National Centre for Ocean Information Services (INCOIS) uses NCMRWF analysis data to force OGCMs and wave models for various operational services. The National Centre for Medium-Range Weather Forecasting (NCMRWF-GFS) analysis has been evaluated in the Indian region over two years (2019-2020). The verification of the analysis was conducted against the RAMA buoy observations, reanalysis, and satellite-based datasets. RAMA(Research Moored Array for African-Asian-Australian Monsoon Analysis and Prediction) buoy observations, available over specific regions at 6-hourly intervals, provided a critical reference point. To evaluate the performance of NCMRWF data, two years (2019, 2020) of NCMRWF analysis data were collocated with RAMA buoy, reanalysis, and satellite-based data. This evaluation was conducted quantitatively using several statistical measures. The statistical errors were estimated using the two years of collocated data for NCMRWF and buoy surface zonal (u) and meridional (v) wind components, wind speed (ws), air temperature(AT) , and humidity (RH or Qa).

## 2. Data and Methods:

To evaluate the accuracy of the NCMRWF analysis products (wind, AT, and RH), we used observations from the Research Moored Array for African–Asian–Australian Monsoon Analysis and Prediction (RAMA) buoys (McPhaden, 2009). Figure 1 illustrates the 19 RAMA buoy station datasets utilized for this study during 2019 and 2020. The comparisons are limited to buoy-measured quantities, including zonal (U) and meridional (V) winds, air temperature (AT), and relative humidity (RH). Additionally, data from NCMRWF-analysis, NCMRWF-reanalysis, ERA5, and CCMP3 are compared with the RAMA buoy data. Conversely, NCMRWF-analysis winds are compared to NCMRWF reanalysis, ERA5 reanalysis, and CCMP3 winds.

Table 1**:** Brief description of different datasets used to evaluate winds for the study

| S.No | Data | source | Temporal resolution | Spatial resolution |
|---|---|---|---|---|
| 1. | NCMRWF Analysis | NCMRWF | 6 hr/daily | 0.25° |
| 2 | RAMA buoy | https://www.pmel.noaa.gov/tao/drupal/disdel/ | Daily | - |
| 3 | ERA5 | https://cds.climate.copernicus.eu/ | 1 hr/daily | 0.25° |
| 4 | NCMRWF Reanalysis | https://rds.ncmrwf.gov.in/ | 1 hr/daily | 0.11° |
| 5 | CCMP3.0 | https://data.remss.com/ccmp/ | 6 hr/daily | 0.25° |

Table 2: Datasets used to evaluate the AT, Humidity:

| S.No | Data | source | Temporal resolution | Spatial resolution | Height(m) |
|---|---|---|---|---|---|
| 1. | NCMRWF Analysis | NCMRWF | 6 hr/daily | 0.25° | 2m |
| 2 | RAMA buoy | https://www.pmel.noaa.gov/tao/drupal/disdel/ | daily | - | 3m |
| 3 | OAFlux | http://apdrc.soest.hawaii.edu/data/data.php | 1 hr/daily | 1° | 2m |
| 4 | ERA5 | https://cds.climate.copernicus.eu/ | 6 hr/daily | 0.25° | 2m |
| 5 | NCMRWF Reanalysis | https://rds.ncmrwf.gov.in/ | 1 hr/daily | 0.11° | 2m |

## 2.1 NCMRWF-Analysis forcing fields:

Two different global Data Assimilation (DA) systems are operational at NCMRWF, i,e NCMUM and GFS. GFS-based GSI-4DEnVar systems provide the initial conditions for the IMD GFS NWP system. This NCEP-based DA system is implemented at NCMRWF and upgraded periodically. The GSI-4DEnVar DA system is a 4-Dimensional Ensemble Variational Data Assimilation System, which uses the ensemble perturbations for estimating the 4-dimensional error covariances during the minimization process of DA. The GSI-

4DEnVar at NCMRWF uses the 80 member ensembles to update the error covariances. This DA system at NCMRWF produces analysis (model initial conditions) at a 6-hourly interval, by running 6 hourly intermittent DA cycles ) (Prasad et al., 2016, John et al., 2016, Sumit Kumar et al., 2018 and Sumit Kumar et al., 2020).

The DA resolution of this system is T576L64 (~25km horizontal over the tropics and 64 hybrid-sigma pressure levels). The 6-hr forecast is used as the background or first guess for the analysis in the DA cycle. The assimilation time window used is +/- 3hr centred on the analysis hour. The 9hr forecast generated from the previous cycle is used for time interpolation of the asynoptic observations within the assimilation time window.

**2.2 NCMRWF IMDAA reanalysis:**

NCMRWF IMDAA (Indian Monsoon Data Assimilation and Analysis) regional reanalysis data is fine horizontal resolution 12 km (N1024L70) upgraded from 17 km resolution (N768L70), which could be helpful to understand the Indian monsoon and its variability. The unified system of the U.K MET office is used in IMDAA. IMDAA uses the Unified Model and is configured with 63 vertical levels extending from near the surface to a height of ~40 km above sea level. The spatial domain of IMDAA extended from 30 E to 120 E and 15 S to 45 N (Rani et al., 2021).

IMDAA uses the 4D-Var data assimilation method of the U.K Met Office based on Rawlins et al. (2007). The observations are available in the 6-h window of each assimilation cycle and are combined with the model background to produce a statistically optimal state of the Atmosphere. The linear perturbation forecast model in the 4D-Var uses a simplified model formulation with a lower grid spacing (~24 km), the a full Unified Model forecast is used to produce the background (~12 km) (Rani et al., 2021). Lateral boundary conditions (ERA-Interim) are taken from the ECMRWF. Sea surface temperature is specified from the Hadley Centre Ice and Sea Surface Temperature dataset version 2 (HadISST2). Soil moisture analysis produced by the Extended Kalman Filter (EKF) based land data assimilation system is used to update the soil moisture fields in every assimilation cycle. The detailed description of the NCMRWF IMDAA reanalysis preparation methodologies is detailed in Rani et al., 2021 (and in https://rds.ncmrwf.gov.in/). The NCMRWF IMDAA reanalysis is called, from here onwards as NCMRWF reanalysis data.

**2.3 ERA5 reanalysis:**

ERA5 is fifth-generation reanalysis data produced using 4D-Var data assimilation and model forecasts in CY41R2 of the ECMWRF Integrated Forecast System (IFS), with 137 hybrid sigma/pressure levels in vertical as well as single (surface) level also. ERA5 data

has been available from 1940 to the present. ERA5 provides hourly, high spatial resolution (0.25° x 0.25°) global climate and atmospheric data. ECMRWF, ERA5 reanalysis (single level) data is utilized in the present study, and data is available from 1940 to the present (Hersbach et al., 2023).

**2.4 Cross-Calibrated Multi-Platform (CCMP3) data:**

Cross-Calibrated Multi-Platform (CCMP3) winds product is the blended satellite product, which is independent of buoy data. No buoy data is included In the CCMP3 product. Scatterometry and imaging spectrometer winds are used in CCMP3 winds by using variational analysis method (ASCAT-B,C version winds are relaxed, used to evaluate the CCMP3 accuracy). Cross-Calibrated Multi-Platform wind product version 3 is generated to provide high-quality wind data that is both spatially and temporally continuous. The primary goal is to bridge any observational gaps to offer a comprehensive understanding of wind patterns in the remote sensing era over both short and long periods. CCMP3 winds data is available from 1993 to 2019 with 0.25 spatial resolution (Carl et al., 2022, Wang et al., 2023).

**2.5 OAFlux data:**

The OAFlux project creates high-quality datasets for air temperature and specific humidity near the sea surface by integrating satellite observations and numerical weather prediction (NWP) model outputs (Yu et al., 2008). Satellite data, including infrared sensors for air temperature and microwave radiometers for specific humidity, provide high-resolution and accurate measurements. These are supplemented by NWP models, such as those from NCEP and ECMWF, which offer comprehensive global coverage and temporal consistency. The integration process employs advanced objective analysis techniques to merge satellite and NWP data, minimizing errors and ensuring a consistent dataset. Buoy data are used for bias correction, comparing satellite and model outputs with accurate in situ observations to adjust any discrepancies. The final data are processed into a 1°×1° resolution grid. This rigorous methodology ensures that the OAFlux data for air temperature and specific humidity are both accurate and reliable, which is crucial for analysing ocean-atmosphere interactions. Buoy data are used for validation purposes but are not directly integrated into the final gridded datasets. OAFlux has provided the data from 1985 to 2022. OAFlux air temperature and specific humidity variables are validated using RAMA buoy data and compared with NCMRWF analysis data

The details of the variables and corresponding datasets used for the study, along with buoy locations, are listed in Table 1 and Table 2.

**2.6 Height corrections:**

For Comparing the model with the observation, the model winds are brought to RAMA buoy height (4m) using empirical logarthimic profile method (Peixoto et al., 1992, Anuradha et al., 2021).

$$U(10) = U(h)\frac{ln(10/z0)}{ln(h/z0)}$$

U(h) is the observed wind speed at height of h(4 m)

u(10) is the estimated wind speed at the 10m height

z0 is the roughness length (m) =1.52 x 10^-4

The statistics in terms of mean, bias, RMSE Pearson Correlation Coefficient, etc., are computed for surface zonal (u) and meridional (v) wind components, Air Temperature, and Specific Humidity.

The air temperature and specific humidity have been converted to '3' m considering stability using the empirical formulation of Monin-Obukhov similarity theory given in Large and Pond (1981, 1982). The corresponding algorithm has been obtained from Kameshwari et al. 2022 and the corresponding python code is obtained from 'https://github.com/kameshwari1991/Meteorology-AWS-data-processing-height-correction-'.

The statistics in terms of mean, bias, RMSE and Pearson Correlation Coefficient etc. are computed for surface zonal (u) and meridional (v) wind components, Air Temperature and Specific Humidity. Error estimation formula are given below in equations form,

$$Mean = \frac{1}{N}\sum_{\{i=1\}}^{\{N\}} X_i \text{ ----------Eq(1)}$$

$$Bias = \frac{1}{N}\sum_{\{i=1\}}^{\{N\}}(M_i - O_i)\text{---------Eq(2)}$$

$$RMSE = \sqrt{\frac{1}{N}\sum_{i=1}^{N}(O_i - M_i)^2}\text{----------Eq(3)}$$

$$Correlation = \frac{\sum(X_i-\bar{X})(Y-\bar{Y})}{\sqrt{\sum(X_i-\bar{X})^2}.\sqrt{\sum(Y_i-\bar{Y})^2}}\text{----------Eq(4)}$$

Here,

N-Total number of Samples, $X_i$-Individual data point, $M_i$-Model-predicted value at sample i, $O_i$-Observed value at sample i, $\bar{X} - is\ mean\ value$ of X, $\bar{Y} - is\ mean\ value$ of Y

The annual and seasonal mean plots are generated at a given resolution. NCMRWF reanalysis data and OAFlux data are regridded to same spatial resolution of the NCMRWF analysis fields, and the spatial bias, standard deviation, and correlation are computed.

## 3. Results:

To evaluate the analysis/forcing fields, we compared the analysis winds with in-situ, reanalysis, and satellite-based data. In Addition to this, we compared the analysis, reanalysis, and satellite-based data with in-situ data. We first compared the NCMRWF analysis, NCMRWF reanalysis, ERA5 reanalysis, and CCMP3 (satellite-based) wind data with in-situ RAMA-buoy winds across the Indian Ocean. The locations of the RAMA buoys are depicted in Figure 1.

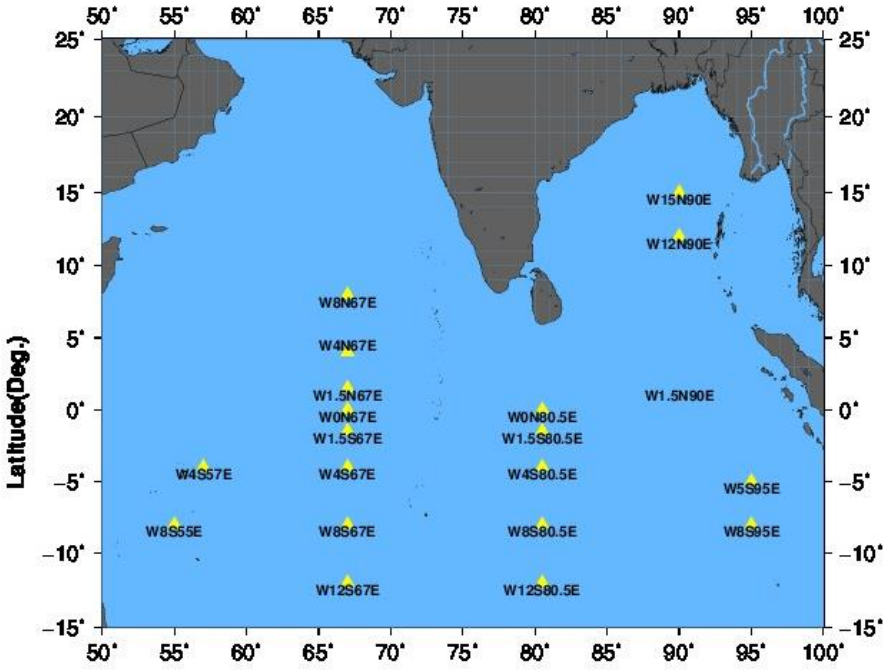


Figure 1: Location map of Rama buoys (Yellow Triangles) used for evaluating NCMRWF Analysis

### 3.1 Validation of winds:

The comparison was carried out for the years 2019 and 2020 (CCMP3 data is only available for 2019). Table 3 shows the statistics i,e bias, RMSE, Correlation Coefficients (CC) etc. The locations of the RAMA buoys and the number of days for which data was available for each buoy during the study period are also shown in Table 3. The spatial and temporal resolution of the analysis fields, reanalysis, and satellite-based data are provided in Table 1, respectively. The time series of zonal, meridional, and wind speeds of all the data sets, along with RAMA buoy winds at 4ºN 67ºE and 1.5ºN 67ºE are shown in Figure 2 and 3. It can be seen that all the products are able to capture the daily variability when compared with buoy observation. These two locations are located in two important regions of the Indian Ocean. One is located in the thermocline dome region where unique open ocean upwelling occurs and witnesses one of the strongest air-sea interaction regions, and another one is in the equatorial Indian Ocean where Wyrtiki Jets presents with the strong inert-

monsoon current. The statistics for all the buoy locations between NCMRWF analysis fields and buoy winds can be seen in Table 3.

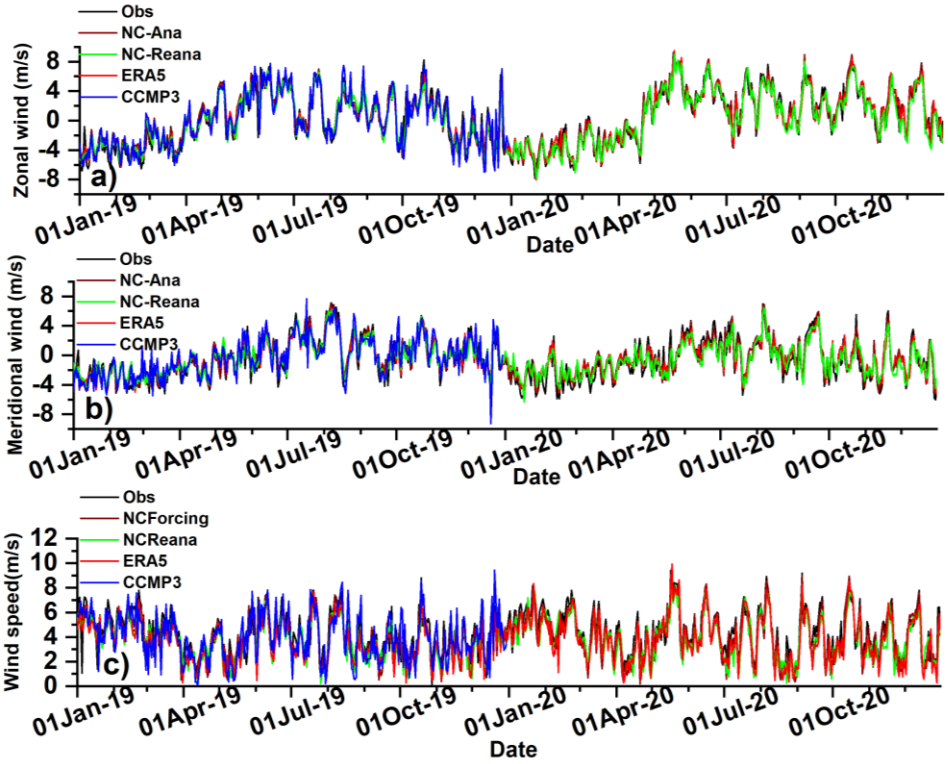


Figure 2: Buoy(obs), NCMRWF analysis (NC-Ana), NCMRWF reanalysis(NC-Reana), ERA5 reanalysis and CCMP3 data a) Zonal, b) Meridional and c) Wind speed at 4°N 67°E

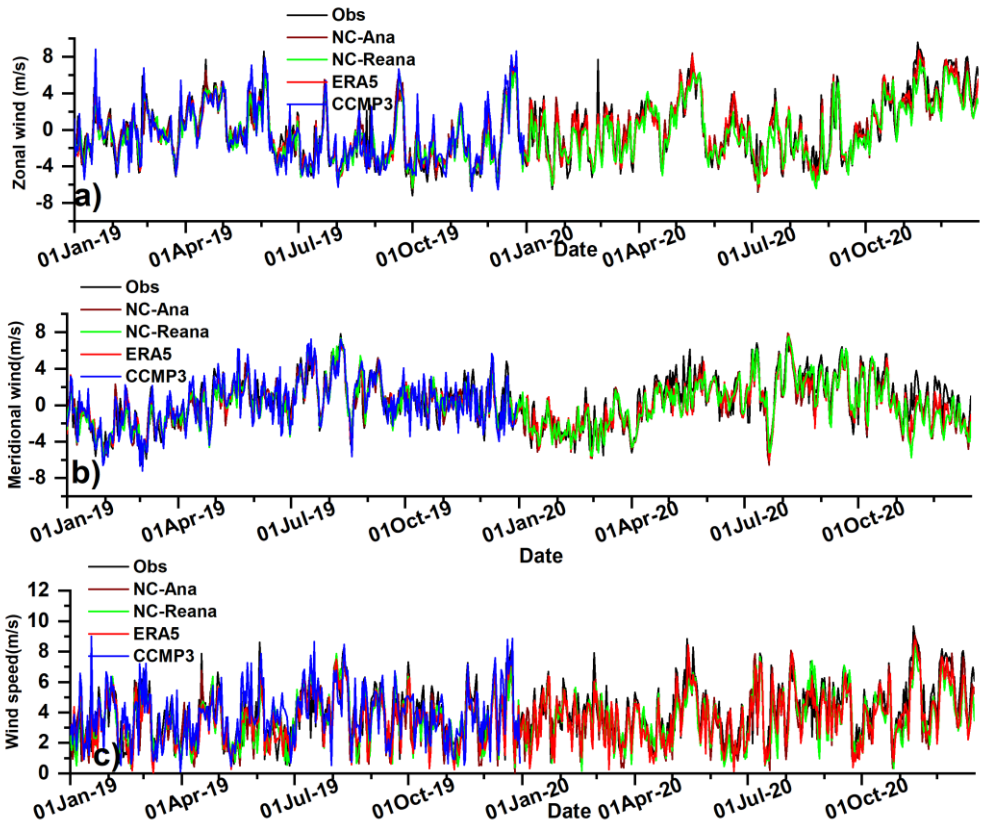


Figure 3: Buoy(obs), NCMRWF analysis (NC-Ana), NCMRWF reanalysis(NC-Reana), ERA5 reanalysis and CCMP3 data a) Zonal, b) Meridional and c) Wind speed at 1.5°N 67°E

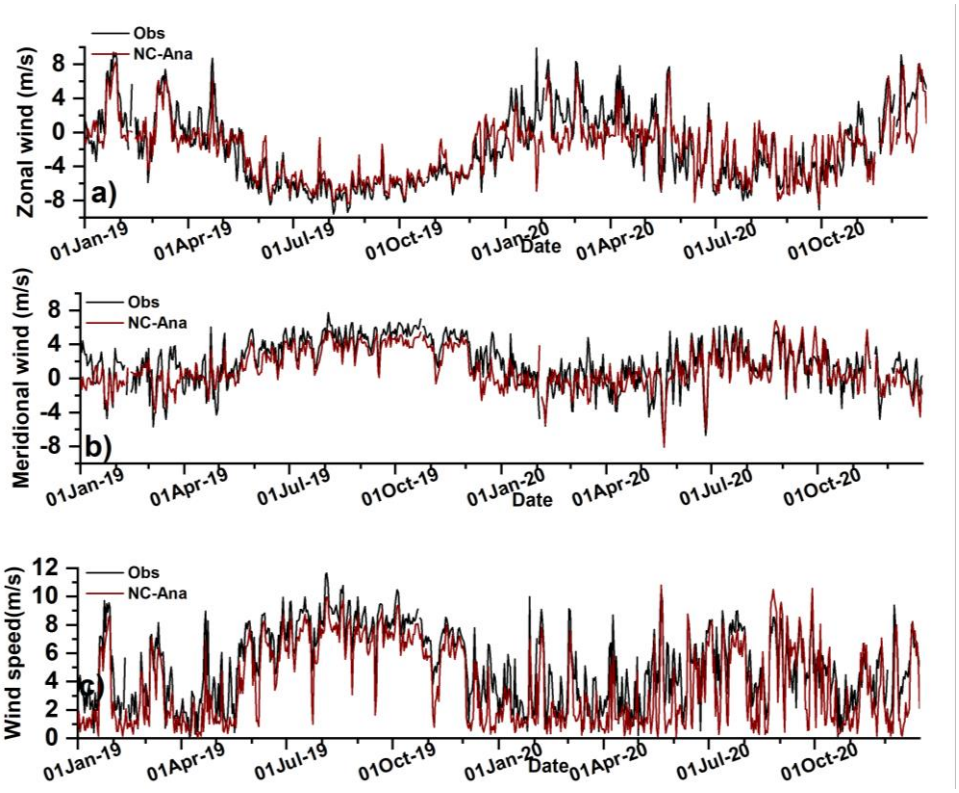


Figure 4: Buoy(obs), NCMRWF analysis (NC-Ana) data a) Zonal, b) Meridional and c) Wind speed at 5°S 95°E

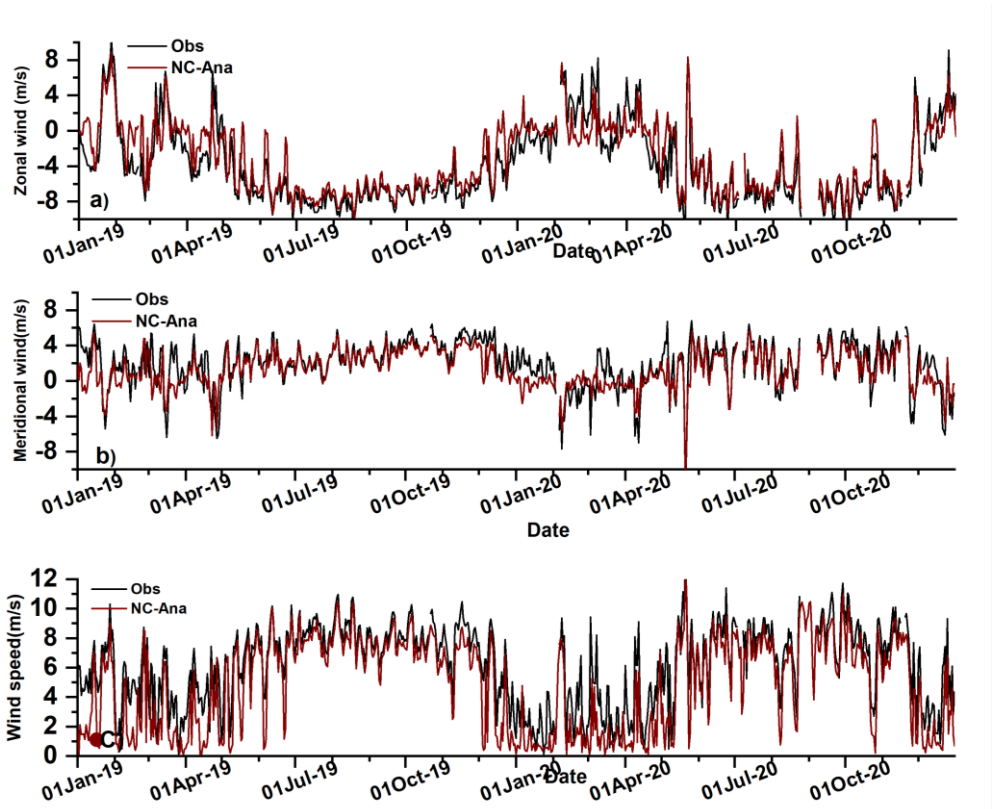


Figure 5: Buoy(obs), NCMRWF analysis (NC-Ana) data a) Zonal, b) Meridional and c) Wind speed at 8°S 95°E

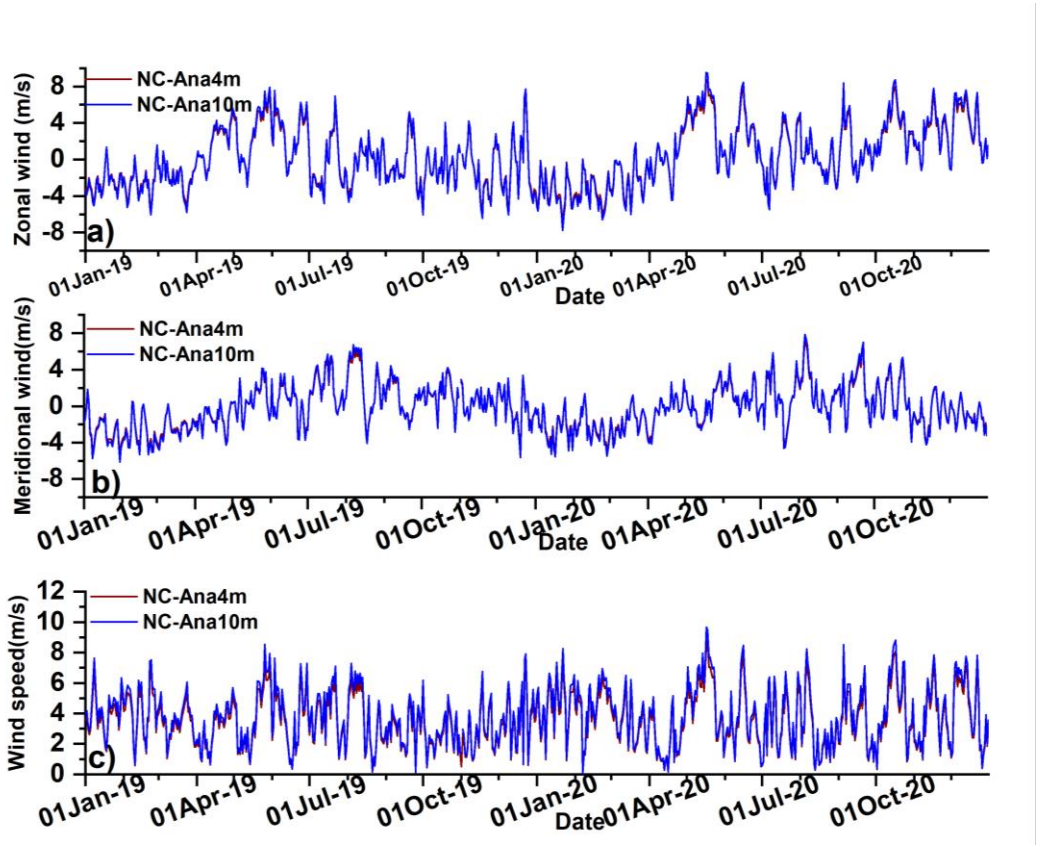


Figure 6: NCMRWF Analysis (NC-Ana): (a) Zonal wind, (b) Meridional wind, and (c) Wind speed at 4 m and 10 m heights, at 1.5°N 67°E.

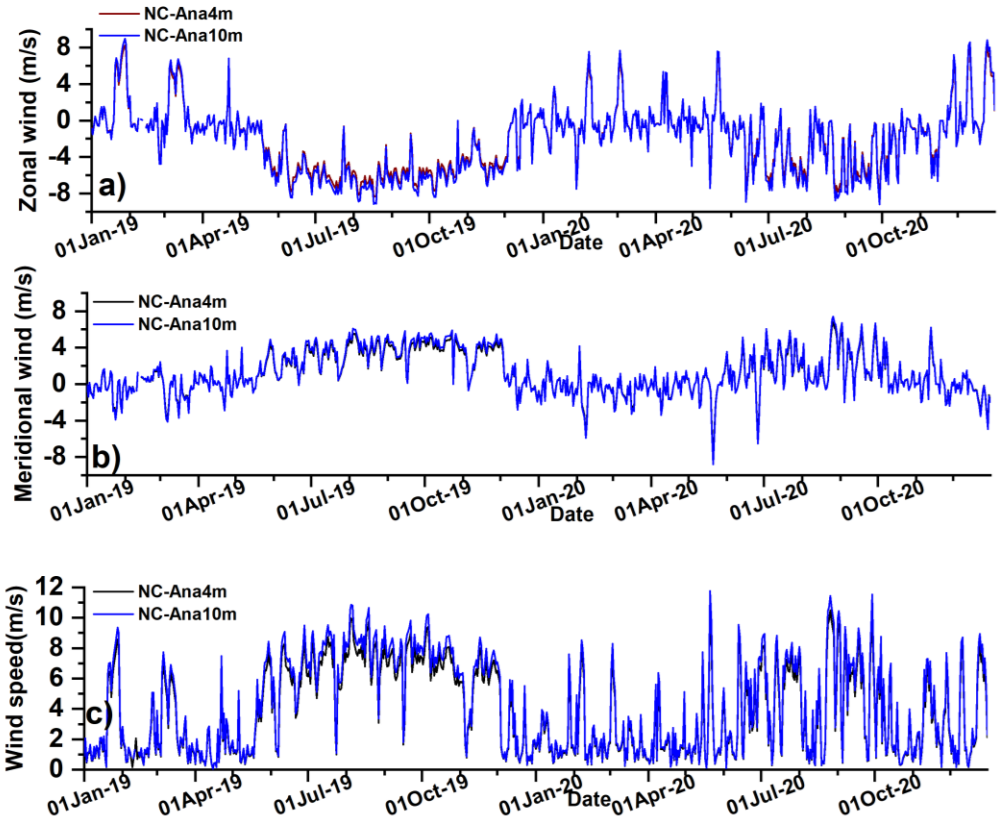


Figure 7: NCMRWF Analysis (NC-Ana): (a) Zonal wind, (b) Meridional wind, and (c) Wind speed at 4 m and 10 m heights, at 5°S 95°E.

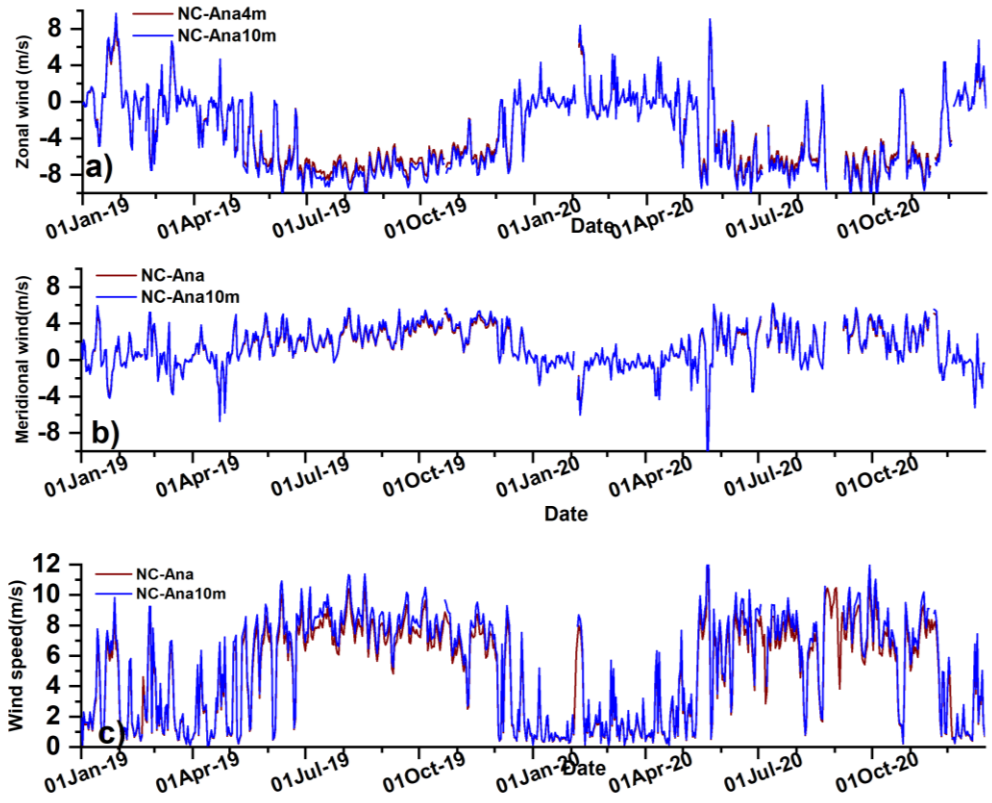


Figure 8: NCMRWF Analysis (NC-Ana): (a) Zonal wind, (b) Meridional wind, and (c) Wind speed at 4 m and 10 m heights, at 8°S 95°E.

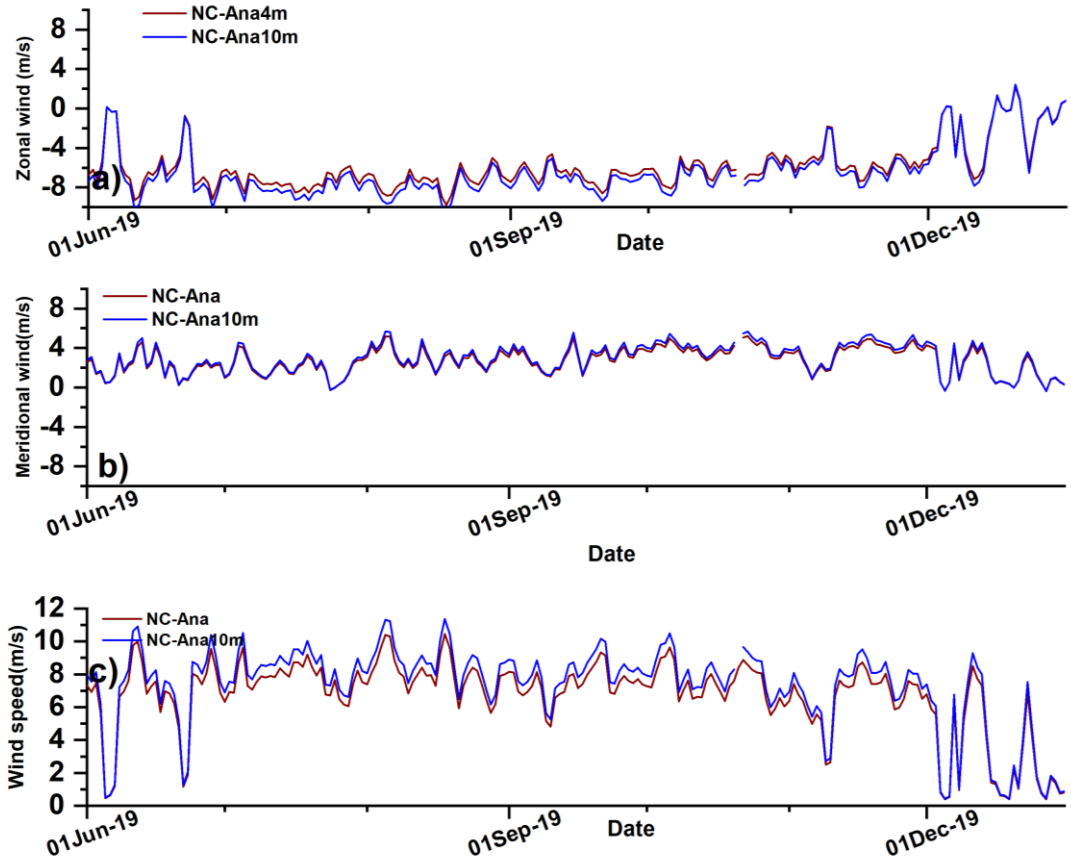


Figure 9: Same as figure 8, zoomed from June to December, 2019.

Figures 4 and 5 show the time series comparisons for the NCMRWF analysis, RAMA buoy observed winds at the locations 5 ºS 95 ºE and 8 ºS 95 ºE. It can be seen although the analysis wind is able to capture the buoy observed variations but, most of the time its unable to capture the higher values. It's worth noting that the height of all the winds has been corrected from 10m to 4m (buoy height). The 4 m and 10 m wind comparisons are shown in Figure 6-9. No significant change of wind between 4 m and 10 m height is observed. However, in zonal wind during summer monsoon time noticeable differences can be seen at 5°S 95°E and 8 ºS 95 ºE. Notably, the winds at 10m tend to be higher than those at 4m due to friction variability, with the difference between the two being minimal.

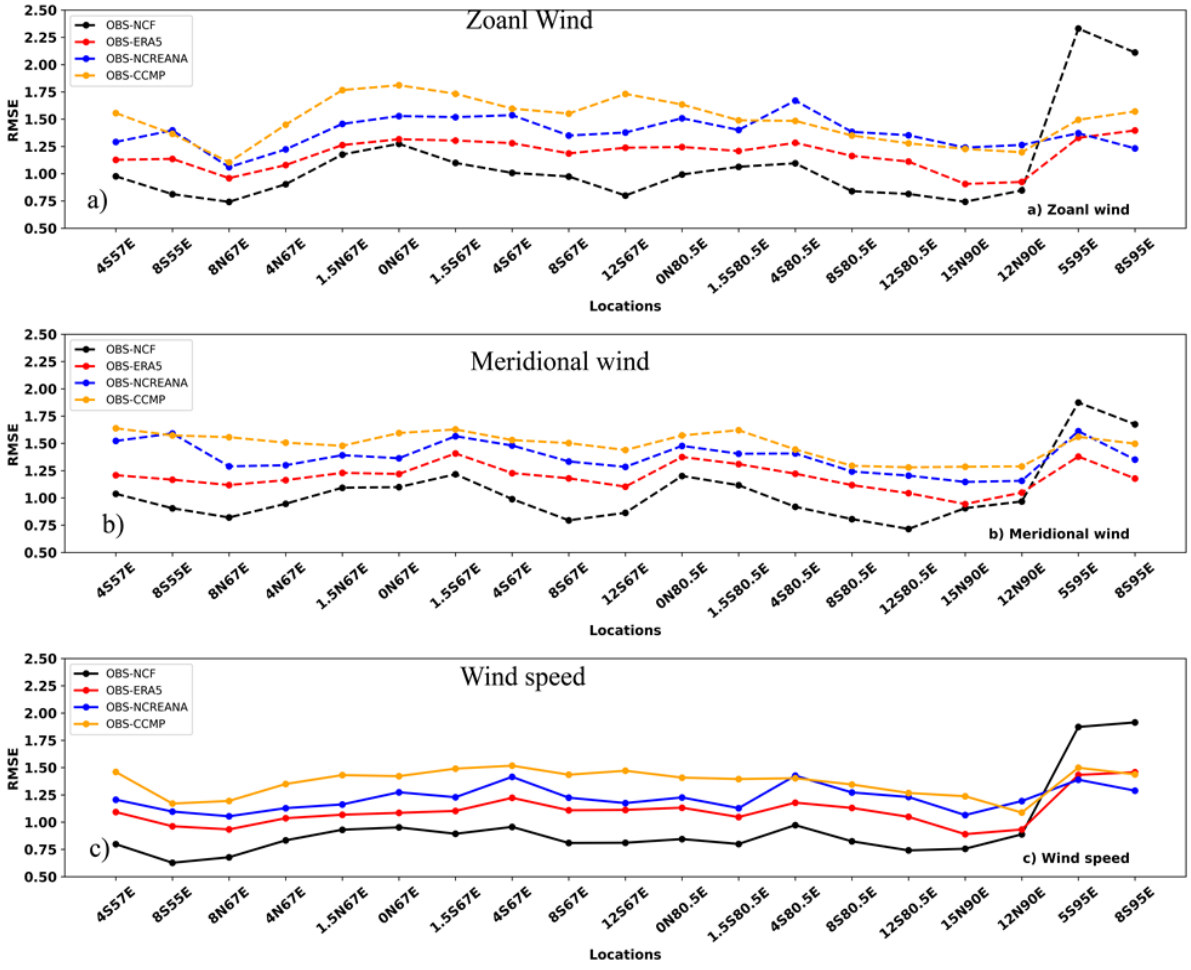


Figure 10: RMSE between Observed Winds with ERA5, NCMRWF Reanalysis, and CCMP Winds: a) Zonal winds, b) Meridional winds, and c) Wind speed.

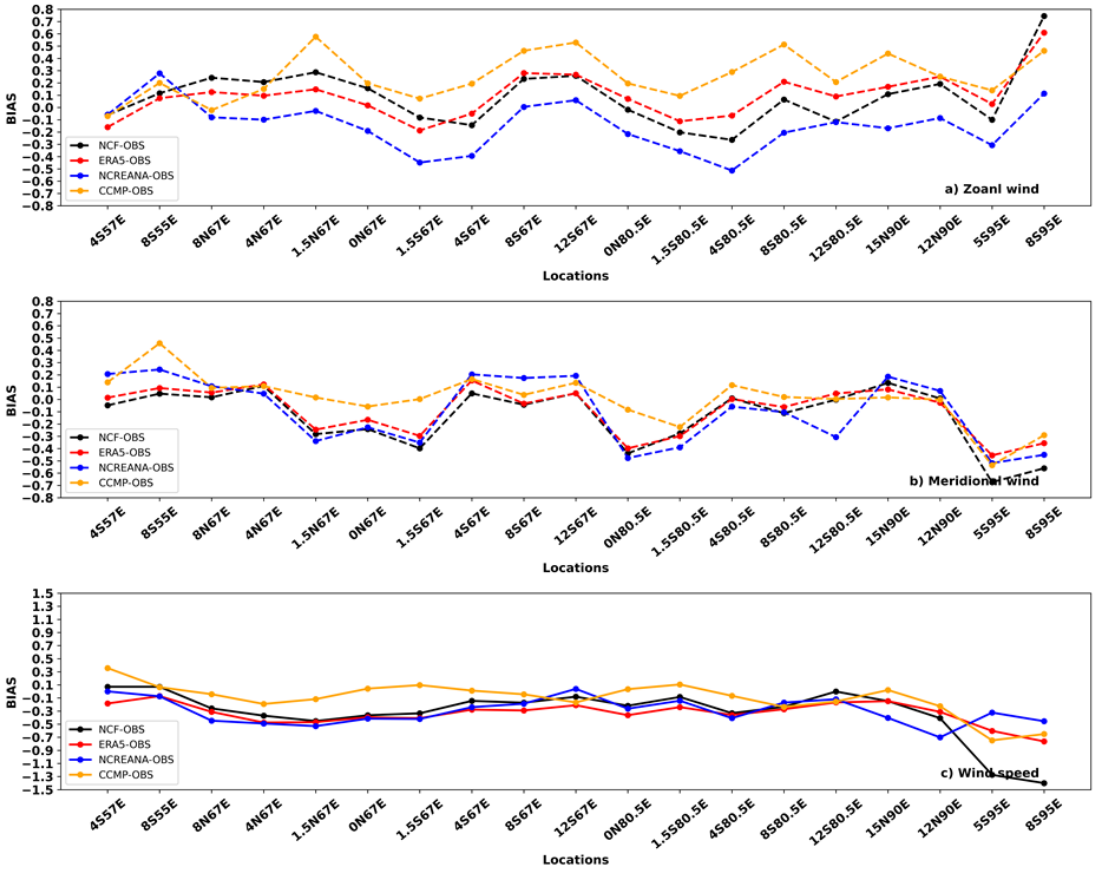


Figure 11: Bias between Observed Winds with ERA5, NCMRWF Reanalysis, and CCMP Winds: a) Zonal winds, b) Meridional winds, and c) Wind speed.

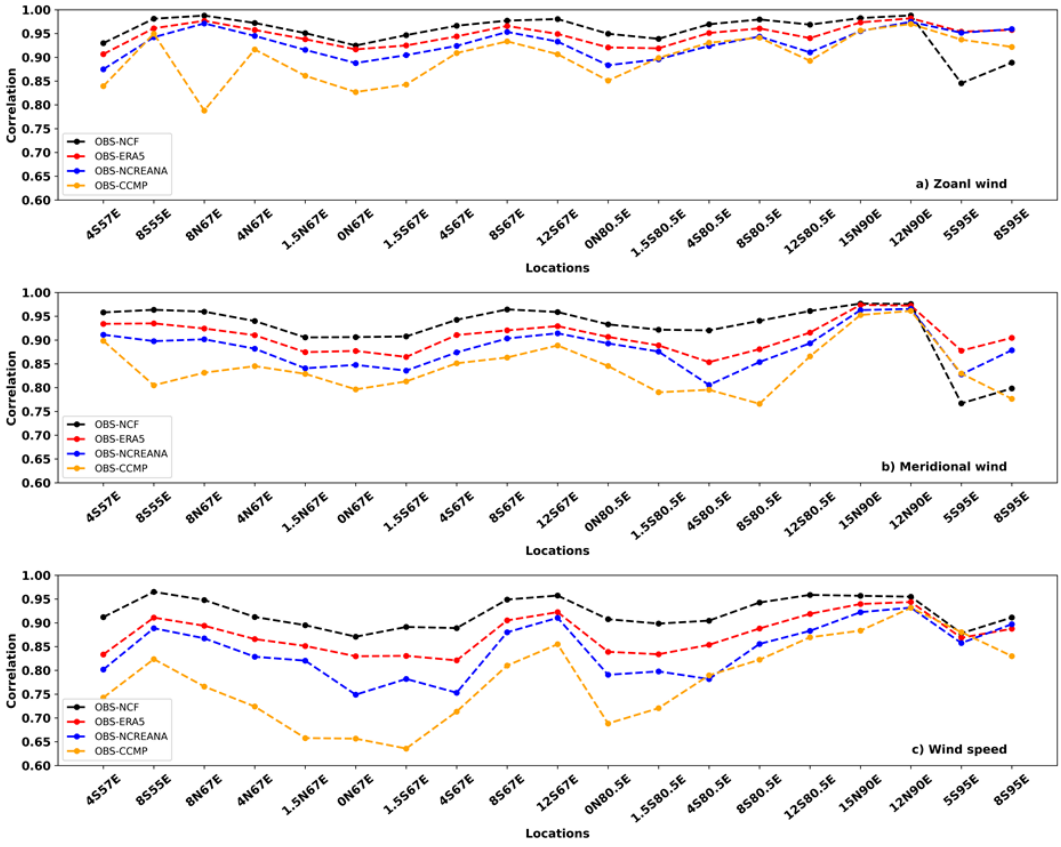


Figure 12: Correlation between Observed Winds with ERA5, NCMRWF Reanalysis, and CCMP3 Winds: a) Zonal winds, b) Meridional winds, and c) Wind speed.

Previous studies have validated the satellite winds (Anuradha et al., 2021), Reanalysis winds (Dora et al., 2019, Rani et al., 2020) with in-situ (OMNI buoy and RAMA buoy) observations, satellite and analysis winds (Sanjib et al., 2009). Offshore buoy wind observations were well matched with satellite winds compared to the coastal buoys; the performance of all reanalysis winds is good and reliable in capturing the direction and speed in the Indian Ocean (Dora et al., 2019). Analysis winds showed good agreement with in-situ and satellite winds at northern Indian Ocean (Bay of Bengal and Arabian Sea) and the equatorial Indian Ocean (Goswami and Rajgopal 2003, Sanjib et al., 2009). Furthermore, precipitation bias correction led to improvements in the analysis winds, reducing the bias to less than 0.5 m/s. The continuous improvement in methodology in data assimilation minimize the deviation between observed and analysis further reanalysis and model winds. Figure 10 displays the root mean square error (RMSE) of NCMRWF reanalysis, ERA5 reanalysis, and CCMP3 datasets for the zonal, meridional, and wind speed components with buoy winds at respective buoy locations. Similarly, biases are depicted in Figure 11, while correlations are illustrated in Figure 12. In the present study, high zonal and meridional wind biases, along with high RMSE, are observed in the southeast equatorial Indian Ocean region between the buoy and NCMRWF analysis winds, compared to the other buoys (Figure 10 & 11) as compared to other reanalysis and satellite-derived products. However, for all other buoy locations, NCMRWF analysis shows the lowest RMSE ( ~ 0.75 m/s), and CCMP shows the highest RMSE ( ~ 1.75 m/s). The opposite trend can be found for the CC plots see Figure 12.

Bias, RMSE, and correlation values between the buoy data and NCMRWF reanalysis, ERA5 reanalysis, and CCMP3 zonal, meridional, and wind speed are presented in Tables 4, 5, and 6, respectively. The NCMRWF analysis wind data demonstrate low RMSE with buoys (less than 1.25 m/s), except for those located in the southeastern equatorial Indian Ocean, specifically at 5°S 95°E and 8°S 95°E, as depicted in Figure 10. After NCMRWF analysis data, NCMRWF reanalysis exhibits the lowest RMSE with the buoys, followed by ERA5 reanalysis and then CCMP3. However, ERA5 reanalysis zonal wind and wind speed data also show higher RMSE at 5°S 95°E and 8°S 95°E compared to the remaining buoys.

The zonal wind bias ranges from -0.3 to 0.3 m/s at 18 out of 19 buoys for NCMRWF analysis zonal wind compared to buoy zonal wind. The exception is the buoy at 8ºS 95ºE, where the bias is 0.74 m/s (Figure 11a). Similarly, the meridional wind bias ranges from -0.3 m/s to 0.1 m/s at 15 out of 19 buoys, except for those at 5°S 95°E (-0.67 m/s), 8ºS 95ºE (-0.56 m/s), 0ºN 80.5ºE (-0.44 m/s), and 1.5S67E (-0.4 m/s) (Figure 11b). The wind speed bias ranges from -0.5 m/s to 0.1 m/s at 17 out of 19 buoy locations, with exceptions at 85°S 95°E

(-1.4 m/s) and 5°S 95°E (-1.2 m/s) (Figure 11c). Alongside NCMRWF analysis, ERA5 reanalysis zonal wind also demonstrates a low bias with buoy zonal wind (Figure 11a), followed by NCMRWF reanalysis and CCMP3 zonal wind with buoy zonal wind. All the datasets, including NCMRWF analysis, NCMRWF reanalysis, ERA5 reanalysis, and CCMP3, exhibit similar values of meridional wind bias with buoy meridional winds (Figure 11b). However, CCMP3 meridional wind exhibits low bias with the buoy at a few locations. At most locations, all the datasets underestimate the wind speed compared to buoy wind speed, resulting in a negative bias. However, the maximum bias between buoy wind speed and NCMRWF analysis, NCMRWF reanalysis, ERA5 reanalysis, and CCMP3 wind speeds are observed at 5ºS 95ºE and 8ºS 95ºE. CCMP3 wind speed exhibits the lowest wind speed bias with the buoy at most buoy locations (Figure 11c).

The correlation of zonal wind (Figure 12a), meridional wind (Figure 12b), and wind speed (Figure 12c) between the buoy and NCMRWF analysis, NCMRWF reanalysis, ERA5 reanalysis, and CCMP3 are shown in Figure 12. Overall, NCMRWF analysis of zonal and meridional winds exhibit a good correlation with buoy zonal, meridional winds. Zonal wind correlation coefficients exceeding 0.9 at 17 out of 19 buoy locations. However, correlations are less than 0.9 at 5°S 95°E and 8°S 95°E, with zonal wind correlation coefficients of 0.84 and 0.88, and meridional wind correlation coefficients of 0.77 and 0.80, respectively. Followed by NCMRWF analysis data, ERA5 reanalysis, NCMRWF reanalysis, and CCMP3 zonal and meridional winds are showing good correlations with buoy zonal and meridional winds (Figure 12a, b). The NCMRWF analysis of meridional wind correlation with buoy meridional wind shows the lowest correlation coefficient of 0.81 at 0ºN 67ºE (shown in Table 3).

The wind speed correlations between the buoy and NCMRWF analysis, NCMRWF reanalysis, ERA5 reanalysis, and CCMP3 are depicted in Figure 12c . NCMRWF analysis wind speed exhibits a high correlation with buoy wind speed at all locations compared to the remaining above data sets; however, the lowest correlation is observed at 0ºN 67ºE and 5ºS 95ºE, with correlation coefficients of 0.87 and 0.88, respectively. Following NCMRWF analysis, wind speed, ERA5, NCMRWF reanalysis, and CCMP3 wind speeds demonstrate good correlations with buoy wind speed. Similar to zonal and meridional wind speeds, CCMP3 exhibits the least correlation with buoy wind speed compared to the other datasets.

NCMRWF analysis data exhibits a strong agreement with buoy data, characterized by low RMSE and high correlation, compared to other reanalysis and remote sensing datasets. However, zonal and meridional winds show higher RMSE and lower correlation at 5ºS 95ºE and 8ºS 95ºE as compared to other products. CCMP3 data demonstrates higher RMSE and lower correlation with buoy data across most locations compared to the other

datasets. Notably, CCMP3 winds do not incorporate buoy data in their generation, potentially contributing to the observed higher RMSE and lower correlation with buoy observations compared to analysis and reanalysis datasets.

Figures 13, 14, and 15 illustrate the frequency distributions of zonal wind, meridional wind, and wind speeds for both buoy and NCMRWF analysis data. The zonal wind frequency distribution mostly shows a skewed distribution pattern (Figure not shown). Over the central BoB a bimodal distribution pattern is observed with two peaks at ~ 4-5 m/s and ~ -3 to -4 m/s (Figure 13, e.g., b)12ºN 90ºE). Similar bi-modal distribution can be seen in meridional wind as well (Figure 14, e.g., b)12ºN 90ºE) . This unique bi-modal distribution could be due to the two monsoon wind patterns during the southwest and northeast monsoon.

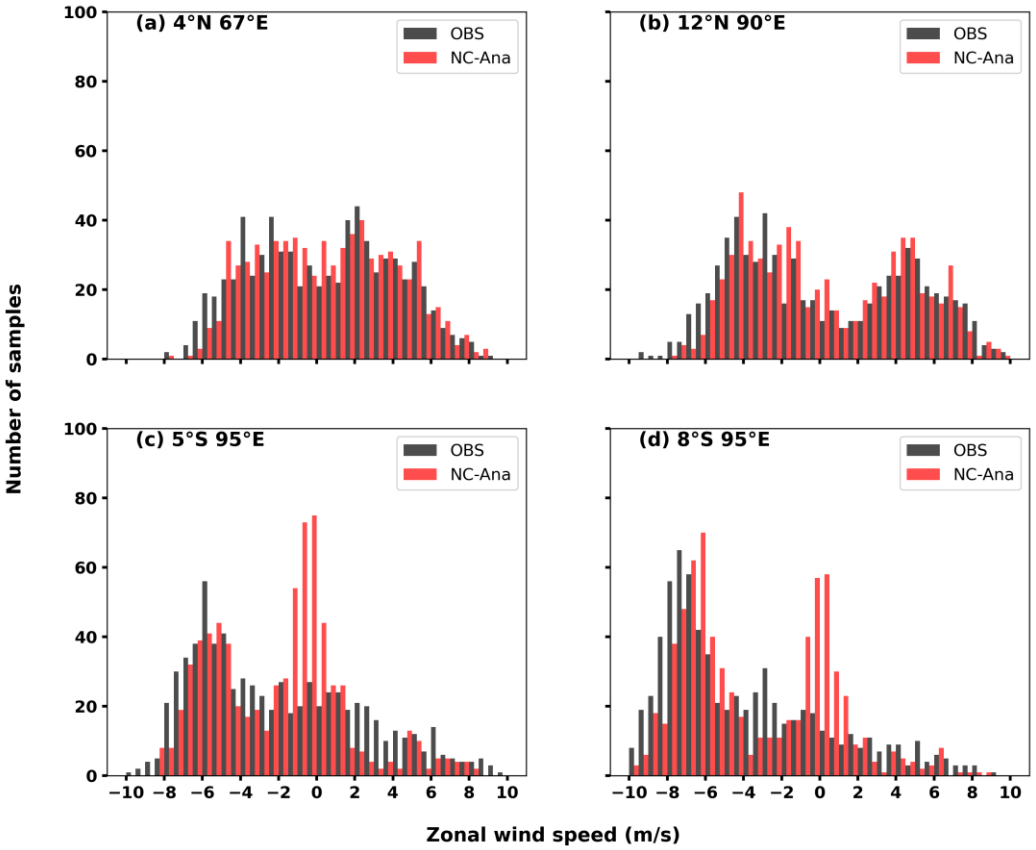


Figure 13: Frequency distribution of RAMA buoy zonal wind speed (black-bar), and NCMRWF-analysis zonal wind speed (red-bar) at a)4°N 67°E, b)12°N 90°E, c)5°S 95°E, d) 8°S 95°E locations

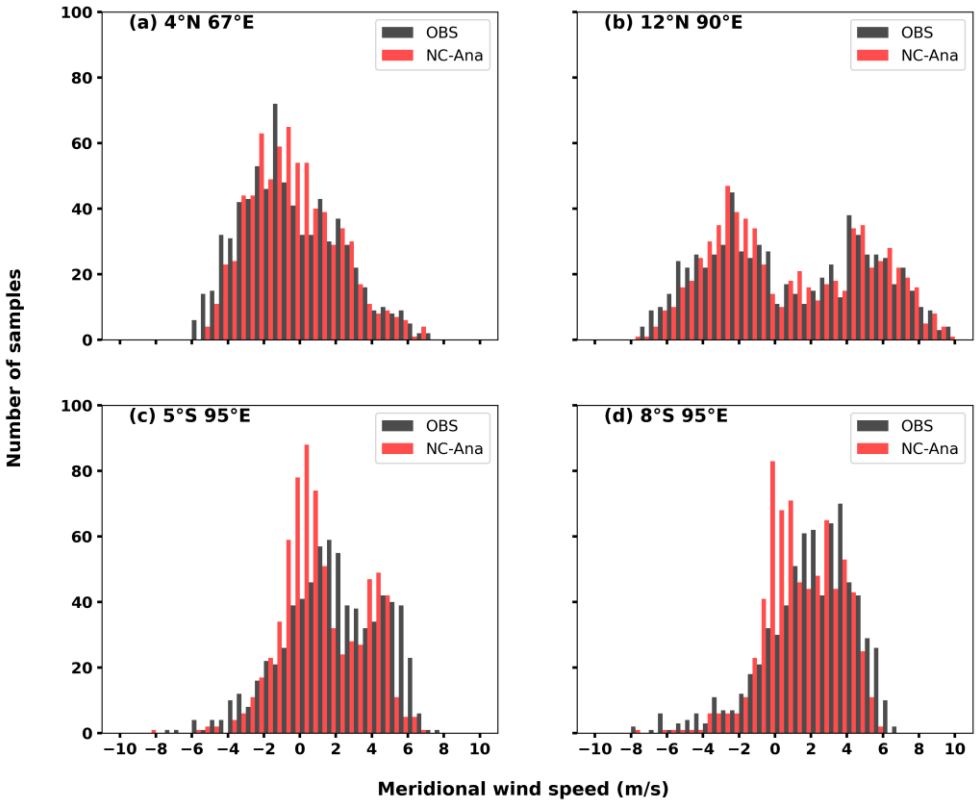


Figure 14: Frequency distribution of RAMA buoy meridional wind speed (black-bar), and NCMRWF- analysis meridional wind speed (red-bar) at a)4°N 67°E, b)12°N 90°E, c)5°S 95°E, d) 8°S 95°E locations

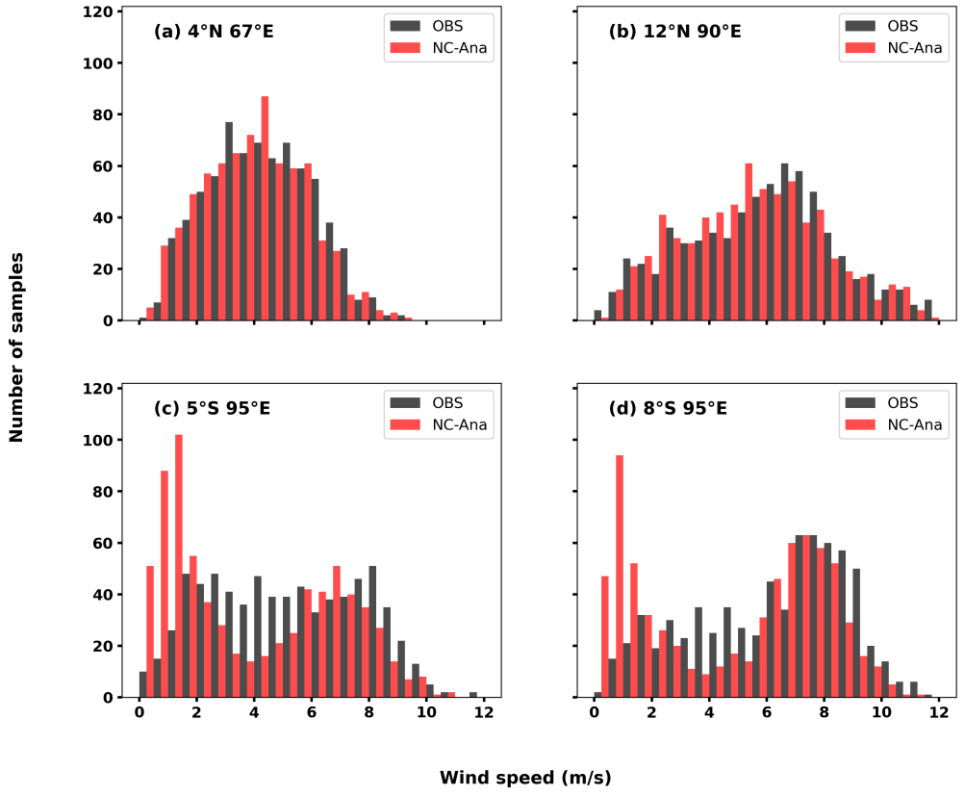


Figure 15: Frequency distribution of RAMA buoy wind speed (black-bar), and NCMRWF- analysis wind speed (red-bar) at a)4°N 67°E, b)12°N 90°E, c)5°S 95°E, d) 8°S 95°E locations

The meridional wind frequency distribution exhibits skewed ness and normality at most locations, as well as a bimodal distribution away from the equator (Figure 15, e.g.,

b)12ºN 90ºE). The buoy zonal wind and NCMRWF analysis zonal wind frequency distributions are well-matched; however, in the southeastern equatorial region at 5ºS 95ºE and 8ºS 95ºE, they exhibit the least agreement. At these locations, within the interval of -2 m/s to 2 m/s, the NCMRWF analysis overestimates the occurrence of zonal wind speeds (Figure 13). Zonal wind speeds greater than 2 m/s and less than -2 m/s are underestimated by the NCMRWF analysis compared to buoy zonal wind occurrences. At the above two locations, the meridional wind frequency distribution exhibits the least agreement between the buoy and NCMRWF analysis meridional winds (Figure 14). The NCMRWF analysis overestimates the occurrence of meridional wind speeds ranging from -2 to 1 m/s at both locations. The least correlation between the buoy and NCMRWF analysis zonal and meridional wind speeds was observed at these two locations.

The buoy wind speed and NCMRWF analysis wind speed frequency distributions are well-matched (Figure 15), with most locations exhibiting a skewed, normal distribution. However, at many locations, the NCMRWF analysis overestimates the occurrence of wind speeds less than 2 m/s, with the largest discrepancy observed at 5ºS 95ºE and 8ºS 95ºE. Despite this, the correlations between buoy wind speed and NCMRWF analysis wind speed at both locations are 0.88 (the lowest correlation compared to the remaining locations) and 0.91, respectively.

Table 3: Statistics between buoy winds and NCMRWF analysis winds. N-number of observations

| | | **Zonal wind** | | | **Meridional wind** | | | **Wind speed** | | | |
|---|---|---|---|---|---|---|---|---|---|---|---|
| **S.No** | **Location** | **RMSE** | **Cor** | **BIAS-NC-UO** | **RMSE** | **Cor** | **BIAS-NC-VO** | **RMSE** | **Cor** | **BIAS-NC-OBS** | **N** |
| 1 | 4°S 57°E | 0.98 | 0.93 | -0.06 | 1.04 | 0.96 | -0.05 | 0.80 | 0.91 | 0.07 | 297 |
| 2 | 8°S 55°E | 0.81 | 0.98 | 0.12 | 0.90 | 0.96 | 0.05 | 0.63 | 0.97 | 0.07 | 431 |
| 3 | 8°N 67°E | 0.74 | 0.99 | 0.24 | 0.82 | 0.96 | 0.02 | 0.68 | 0.95 | -0.26 | 463 |
| 4 | 4°N 67°E | 0.90 | 0.97 | 0.21 | 0.95 | 0.94 | 0.11 | 0.83 | 0.91 | -0.37 | 729 |
| 5 | 1.5°N 67°E | 1.18 | 0.95 | 0.29 | 1.09 | 0.91 | -0.28 | 0.93 | 0.90 | -0.45 | 730 |
| 6 | 0°N 67°E | 1.27 | 0.92 | 0.16 | 1.10 | 0.91 | -0.24 | 0.95 | 0.87 | -0.36 | 592 |
| 7 | 1.5°S 67°E | 1.10 | 0.95 | -0.08 | 1.22 | 0.91 | -0.40 | 0.89 | 0.89 | -0.33 | 730 |
| 8 | 4°S 67°E | 1.01 | 0.97 | -0.14 | 0.99 | 0.94 | 0.05 | 0.96 | 0.89 | -0.14 | 678 |
| 9 | 8°S 67°E | 0.97 | 0.98 | 0.23 | 0.79 | 0.96 | -0.04 | 0.81 | 0.95 | -0.17 | 731 |
| 10 | 12°S 67°E | 0.80 | 0.98 | 0.26 | 0.86 | 0.96 | 0.05 | 0.81 | 0.96 | -0.08 | 240 |
| 11 | 0°N 80.5°E | 0.99 | 0.95 | -0.02 | 1.20 | 0.93 | -0.44 | 0.84 | 0.91 | -0.22 | 444 |
| 12 | 1.5°S 80.5°E | 1.06 | 0.94 | -0.20 | 1.12 | 0.92 | -0.28 | 0.80 | 0.90 | -0.09 | 440 |
| 13 | 4°S 80.5°E | 1.10 | 0.97 | -0.26 | 0.92 | 0.92 | 0.01 | 0.97 | 0.90 | -0.33 | 730 |
| 14 | 8°S 80.5°E | 0.84 | 0.98 | 0.06 | 0.81 | 0.94 | -0.11 | 0.82 | 0.94 | -0.23 | 462 |
| 15 | 12°S 80.5°E | 0.81 | 0.97 | -0.12 | 0.72 | 0.96 | 0.00 | 0.74 | 0.96 | 0.00 | 730 |
| 16 | 15°N 90°E | 0.74 | 0.98 | 0.11 | 0.91 | 0.98 | 0.14 | 0.76 | 0.96 | -0.15 | 613 |
| 17 | 12°N 90°E | 0.85 | 0.99 | 0.19 | 0.97 | 0.98 | 0.01 | 0.89 | 0.95 | -0.41 | 692 |
| 20 | 5°S 95°E | 2.33 | 0.85 | -0.10 | 1.87 | 0.77 | -0.67 | 1.87 | 0.88 | -1.27 | 722 |
| 21 | 8°S 95°E | 2.11 | 0.89 | 0.74 | 1.67 | 0.80 | -0.56 | 1.91 | 0.91 | -1.40 | 709 |

Table 4: Statistics between buoy winds and NCMRWF reanalysis winds. N-number of observations

| | | Zonal wind | | | Meridional wind | | | Wind speed | | | |
|---|---|---|---|---|---|---|---|---|---|---|---|
| S.No | Location | RMSE | Cor | BIAS-NCR-UO | RMSE | Cor | BIAS-NCR-VO | RMSE | Cor | BIAS-NCR-Obs | N |
| 1 | 4°S 57°E | 1.29 | 0.87 | -0.06 | 1.52 | 0.91 | 0.21 | 1.21 | 0.80 | 0.00 | 297 |
| 2 | 8°S 55°E | 1.40 | 0.94 | 0.28 | 1.59 | 0.90 | 0.24 | 1.10 | 0.89 | -0.08 | 431 |
| 3 | 8°N 67°E | 1.06 | 0.97 | -0.08 | 1.29 | 0.90 | 0.11 | 1.05 | 0.87 | -0.45 | 463 |
| 4 | 4°N 67°E | 1.22 | 0.94 | -0.10 | 1.30 | 0.88 | 0.05 | 1.13 | 0.83 | -0.49 | 729 |
| 5 | 1.5°N 67°E | 1.46 | 0.92 | -0.03 | 1.39 | 0.84 | -0.34 | 1.16 | 0.82 | -0.53 | 730 |
| 6 | 0°N 67°E | 1.53 | 0.89 | -0.19 | 1.36 | 0.85 | -0.23 | 1.27 | 0.75 | -0.42 | 592 |
| 7 | 1.5°S 67°E | 1.52 | 0.90 | -0.45 | 1.57 | 0.84 | -0.35 | 1.23 | 0.78 | -0.42 | 730 |
| 8 | 4°S 67°E | 1.54 | 0.92 | -0.39 | 1.48 | 0.87 | 0.20 | 1.42 | 0.75 | -0.24 | 678 |
| 9 | 8°S 67°E | 1.35 | 0.95 | 0.00 | 1.33 | 0.90 | 0.17 | 1.22 | 0.88 | -0.19 | 731 |
| 10 | 12°S 67°E | 1.38 | 0.93 | 0.06 | 1.28 | 0.91 | 0.19 | 1.17 | 0.91 | 0.04 | 240 |
| 11 | 0°N 80.5°E | 1.51 | 0.88 | -0.22 | 1.48 | 0.89 | -0.48 | 1.23 | 0.79 | -0.26 | 444 |
| 12 | 1.5°S 80.5°E | 1.40 | 0.90 | -0.36 | 1.41 | 0.88 | -0.39 | 1.13 | 0.80 | -0.14 | 440 |
| 13 | 4°S 80.5°E | 1.67 | 0.92 | -0.51 | 1.41 | 0.81 | -0.06 | 1.43 | 0.78 | -0.41 | 730 |
| 14 | 8°S 80.5°E | 1.38 | 0.94 | -0.20 | 1.24 | 0.85 | -0.10 | 1.27 | 0.86 | -0.17 | 462 |
| 15 | 12°S 80.5°E | 1.35 | 0.91 | -0.12 | 1.20 | 0.89 | -0.31 | 1.23 | 0.88 | -0.12 | 730 |
| 16 | 15°N 90°E | 1.24 | 0.96 | -0.17 | 1.15 | 0.96 | 0.19 | 1.06 | 0.92 | -0.40 | 613 |
| 17 | 12°N 90°E | 1.26 | 0.97 | -0.09 | 1.16 | 0.97 | 0.07 | 1.19 | 0.93 | -0.70 | 692 |
| 20 | 5°S 95°E | 1.37 | 0.95 | -0.31 | 1.61 | 0.83 | -0.52 | 1.39 | 0.86 | -0.32 | 722 |
| 21 | 8°S 95°E | 1.23 | 0.96 | 0.11 | 1.35 | 0.88 | -0.45 | 1.29 | 0.90 | -0.46 | 709 |

Table 5: Statistics between buoy winds and ERA5 reanalysis winds. N-number of observations

| | | Zonal wind | | | Meridional wind | | | Wind speed | | | |
|---|---|---|---|---|---|---|---|---|---|---|---|
| S.NO | Location | RMSE | Cor | BIAS-E5-UO | RMSE | Cor | BIAS-E5-VO | RMSE | Cor | BIAS-ERA5-Obs | N |
| 1 | 4°S 57°E | 1.13 | 0.91 | -0.16 | 1.21 | 0.93 | 0.01 | 1.09 | 0.83 | -0.18 | 297 |
| 2 | 8°S 55°E | 1.14 | 0.96 | 0.08 | 1.17 | 0.94 | 0.09 | 0.96 | 0.91 | -0.07 | 431 |
| 3 | 8°N 67°E | 0.96 | 0.98 | 0.13 | 1.12 | 0.92 | 0.06 | 0.93 | 0.89 | -0.31 | 463 |
| 4 | 4°N 67°E | 1.08 | 0.96 | 0.10 | 1.16 | 0.91 | 0.12 | 1.04 | 0.87 | -0.48 | 729 |
| 5 | 1.5°N 67°E | 1.26 | 0.94 | 0.15 | 1.23 | 0.87 | -0.25 | 1.07 | 0.85 | -0.47 | 730 |
| 6 | 0°N 67°E | 1.32 | 0.92 | 0.02 | 1.22 | 0.88 | -0.17 | 1.08 | 0.83 | -0.39 | 592 |
| 7 | 1.5°S 67°E | 1.30 | 0.92 | -0.19 | 1.41 | 0.86 | -0.30 | 1.10 | 0.83 | -0.41 | 730 |
| 8 | 4°S 67°E | 1.28 | 0.94 | -0.05 | 1.23 | 0.91 | 0.15 | 1.22 | 0.82 | -0.28 | 678 |
| 9 | 8°S 67°E | 1.19 | 0.97 | 0.28 | 1.18 | 0.92 | -0.03 | 1.11 | 0.91 | -0.29 | 731 |
| 10 | 12°S 67°E | 1.24 | 0.95 | 0.27 | 1.10 | 0.93 | 0.05 | 1.11 | 0.92 | -0.21 | 240 |
| 11 | 0°N 80.5°E | 1.24 | 0.92 | 0.07 | 1.38 | 0.91 | -0.40 | 1.13 | 0.84 | -0.36 | 444 |
| 12 | 1.5°S 80.5°E | 1.21 | 0.92 | -0.11 | 1.31 | 0.89 | -0.30 | 1.05 | 0.83 | -0.24 | 440 |
| 13 | 4°S 80.5°E | 1.28 | 0.95 | -0.07 | 1.22 | 0.85 | 0.00 | 1.18 | 0.85 | -0.36 | 730 |
| 14 | 8°S 80.5°E | 1.16 | 0.96 | 0.21 | 1.12 | 0.88 | -0.06 | 1.13 | 0.89 | -0.27 | 462 |
| 15 | 12°S 80.5°E | 1.11 | 0.94 | 0.09 | 1.04 | 0.92 | 0.05 | 1.05 | 0.92 | -0.17 | 730 |
| 16 | 15°N 90°E | 0.91 | 0.97 | 0.17 | 0.94 | 0.97 | 0.08 | 0.89 | 0.94 | -0.15 | 613 |
| 17 | 12°N 90°E | 0.92 | 0.98 | 0.25 | 1.05 | 0.97 | -0.03 | 0.93 | 0.94 | -0.31 | 692 |
| 20 | 5°S 95°E | 1.33 | 0.95 | 0.03 | 1.38 | 0.88 | -0.46 | 1.43 | 0.87 | -0.60 | 722 |
| 21 | 8°S 95°E | 1.40 | 0.96 | 0.61 | 1.18 | 0.90 | -0.36 | 1.46 | 0.89 | -0.76 | 709 |

Table 6:Statistics between buoy winds and CCMP reanalysis winds. N-number of observations

| | | Zonal wind | | | Meridional wind | | | Wind speed | | | |
|---|---|---|---|---|---|---|---|---|---|---|---|
| S.No | Location | RMSE | Cor | BIAS-UCMP-UO | RMSE | Cor | BIAS-VCMP-VO | RMSE | Cor | BIAS-CCMP-Obs | N |
| 1 | 4°S 57°E | 1.56 | 0.84 | -0.07 | 1.64 | 0.90 | 0.14 | 1.46 | 0.74 | 0.36 | 297 |
| 2 | 8°S 55°E | 1.36 | 0.95 | 0.20 | 1.57 | 0.80 | 0.46 | 1.17 | 0.82 | 0.06 | 431 |
| 3 | 8°N 67°E | 1.10 | 0.79 | -0.02 | 1.56 | 0.83 | 0.09 | 1.19 | 0.77 | -0.04 | 463 |
| 4 | 4°N 67°E | 1.45 | 0.92 | 0.15 | 1.51 | 0.85 | 0.11 | 1.35 | 0.72 | -0.19 | 729 |
| 5 | 1.5°N 67°E | 1.77 | 0.86 | 0.58 | 1.48 | 0.83 | 0.02 | 1.43 | 0.66 | -0.12 | 730 |
| 6 | 0°N 67°E | 1.81 | 0.83 | 0.20 | 1.59 | 0.80 | -0.06 | 1.42 | 0.66 | 0.04 | 592 |
| 7 | 1.5°S 67°E | 1.73 | 0.84 | 0.07 | 1.63 | 0.81 | 0.00 | 1.49 | 0.64 | 0.10 | 730 |
| 8 | 4°S 67°E | 1.60 | 0.91 | 0.19 | 1.53 | 0.85 | 0.17 | 1.52 | 0.71 | 0.01 | 678 |
| 9 | 8°S 67°E | 1.55 | 0.93 | 0.46 | 1.50 | 0.86 | 0.04 | 1.43 | 0.81 | -0.04 | 731 |
| 10 | 12°S 67°E | 1.73 | 0.91 | 0.53 | 1.44 | 0.89 | 0.14 | 1.47 | 0.85 | -0.17 | 240 |
| 11 | 0°N 80.5°E | 1.63 | 0.85 | 0.20 | 1.57 | 0.85 | -0.08 | 1.41 | 0.69 | 0.03 | 444 |
| 12 | 1.5°S 80.5°E | 1.49 | 0.90 | 0.09 | 1.62 | 0.79 | -0.22 | 1.40 | 0.72 | 0.11 | 440 |
| 13 | 4°S 80.5°E | 1.48 | 0.93 | 0.29 | 1.44 | 0.80 | 0.12 | 1.40 | 0.79 | -0.07 | 730 |
| 14 | 8°S 80.5°E | 1.35 | 0.94 | 0.51 | 1.29 | 0.77 | 0.02 | 1.34 | 0.82 | -0.24 | 462 |
| 15 | 12°S 80.5°E | 1.28 | 0.89 | 0.21 | 1.28 | 0.87 | 0.00 | 1.27 | 0.87 | -0.16 | 730 |
| 16 | 15°N 90°E | 1.23 | 0.96 | 0.44 | 1.29 | 0.95 | 0.02 | 1.24 | 0.88 | 0.02 | 613 |
| 17 | 12°N 90°E | 1.20 | 0.97 | 0.25 | 1.29 | 0.96 | 0.00 | 1.09 | 0.93 | -0.23 | 692 |
| 20 | 5°S 95°E | 1.49 | 0.94 | 0.14 | 1.56 | 0.83 | -0.54 | 1.50 | 0.88 | -0.75 | 722 |
| 21 | 8°S 95°E | 1.57 | 0.92 | 0.46 | 1.50 | 0.78 | -0.29 | 1.44 | 0.83 | -0.65 | 709 |

## 3.2 Spatial variability of winds:

In this section, we show how NCMRWF analysis data varies spatially with reanalysis and blended remote sensing data. NCMRWF analysis, NCMRWF, and ERA5 reanalysis data are available for 2019 and 2020, while CCMP3 is available only for 2019; hence, 2019 data is presented for comparison. During 2019, over the study region, annual average wind speed and wind direction from the above-mentioned data sources exhibited similar patterns (Figure 16), with CCMP slightly stronger than other products. The annual average winds reveal that south-easterly trade winds dominate in the southern Indian Ocean from 15ºS to 5ºS, originating at the Mascarene High (at 30ºS). The annual average wind speed indicates that high wind speeds are observed south of 10ºS, north of the equator to 15ºN along the Somalia coast, Arabian Sea, and southern Bay of Bengal, with the lowest wind speed observed at the equatorial belt and the north Sumatra coast.

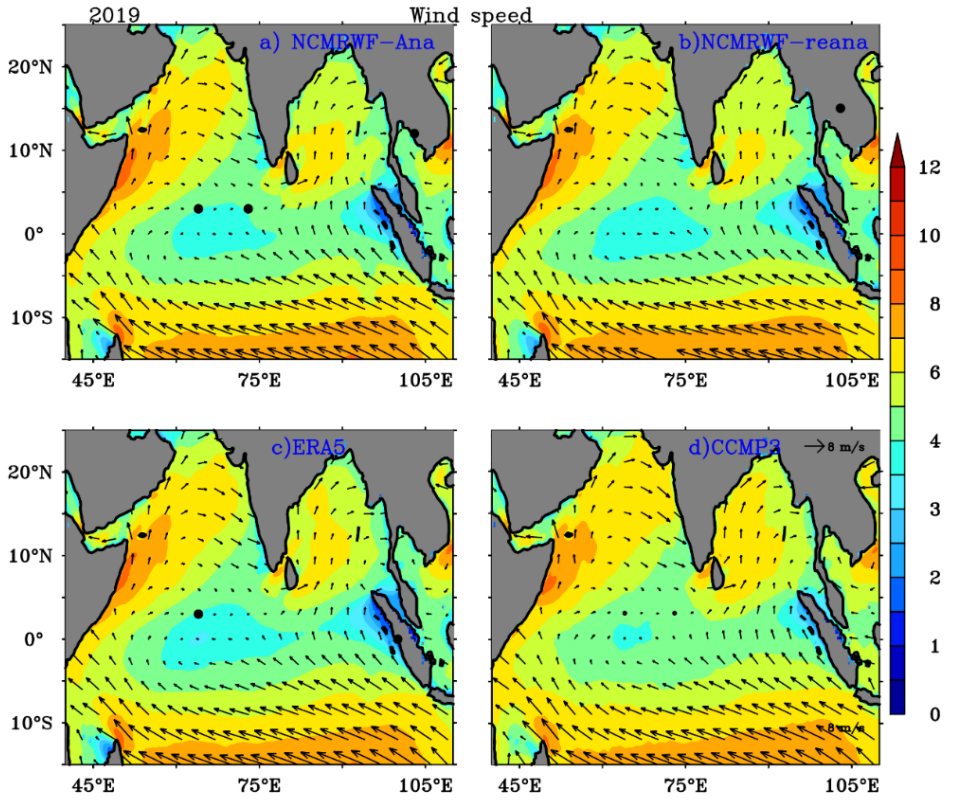


Figure 16: Annual averaged wind speed overlaid with wind vectors for 2019: (a) NCMRWF Analysis, (b) NCMRWF Reanalysis, (c) ERA5, and (d) CCMP3.

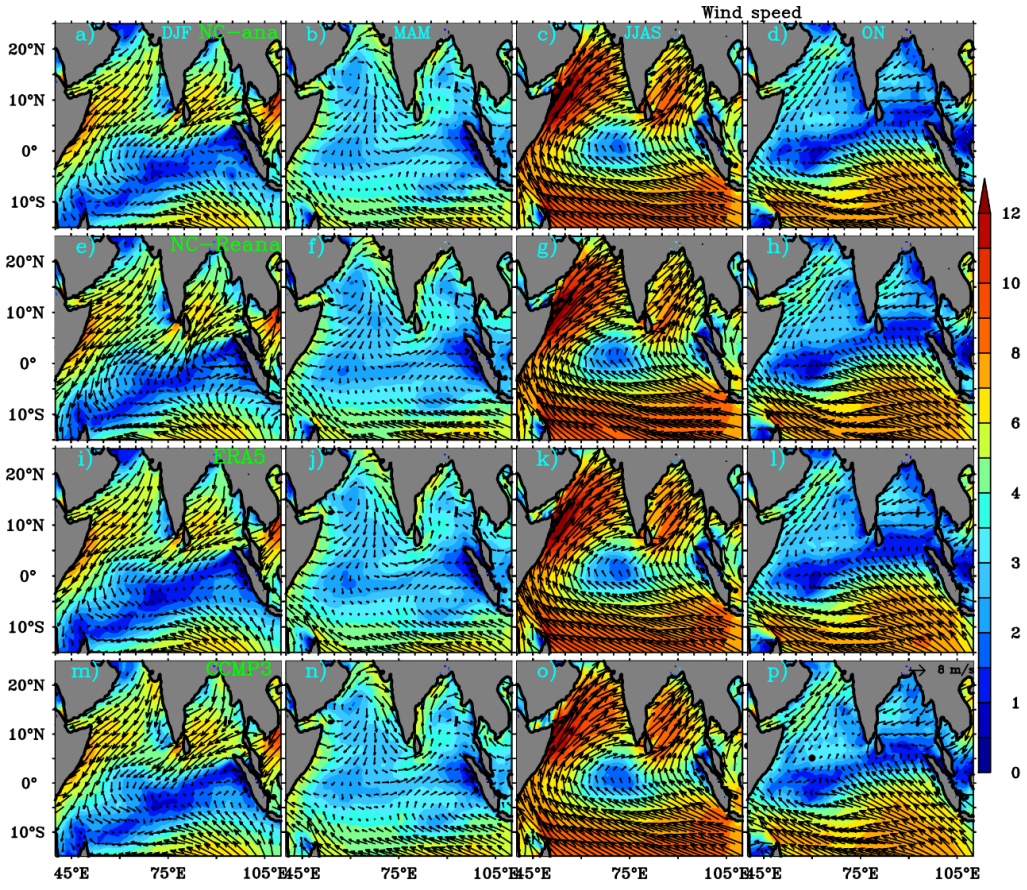


Figure 17: Seasonal averaged wind speed overlaid with wind vectors of NCMRWF analysis (a-d), NCMRWF reanalysis (e-h), ERA5 reanalysis (i-l), and CCMP3 (m-p) data.

All four datasets exhibit the same aforementioned results. In the inter-comparison of NCMRWF-analysis (Figure 16a) and NCMRWF reanalysis, ERA5 reanalysis, and CCMP3 (Figure 16b-16d), similar wind speeds are observed. ERA5 and CCMP3 show higher wind speeds at the Bay of Bengal compared to NCMRWF analysis and reanalysis. CCMP3 wind speed indicates higher wind speeds than NCMRWF analysis, NCMRWF reanalysis, and ERA5 in the equatorial region (60ºE-75ºE, 0ºN to 5ºN/5ºS). To determine whether the variations observed in the annual comparison are present at the seasonal scale, we conducted a seasonal analysis comparison (Figure 17). No significant difference is found on the seasonal wind pattern among the products other than annual mean comparison (Figure 17). Figure 18 shows the seasonal wind speed bias of NCMRWF analysis compared with NCMRWF reanalysis, ERA5, and CCMP3. CCMP3 exhibits a higher bias compared to NCMRWF and ERA5 reanalysis with respect to NCMRWF analysis wind speed. All datasets show a high bias during the southwest monsoon season.

The zonal and meridional wind speed RMSE, bias, and correlation between NCMRWF analysis and NCMRWF and ERA5 reanalysis are depicted in Figure 19, 20. NCMRWF reanalysis and ERA5 demonstrate good correlation with NCMRWF analysis data, whereas they exhibit the least correlation with CCMP3 data. In summary, when compared with NCMRWF analysis data, NCMRWF reanalysis data exhibit high RMSE, whereas CCMP3 data (Figure not shown) show low RMSE. Similarly, NCMRWF reanalysis and ERA5 wind speed display positive bias, while CCMP3 exhibits a negative bias over the dominant region. Furthermore, ERA5 and NCMRWF reanalysis demonstrate high correlation, whereas CCMP3 shows the least correlation with NCMRWF analysis data. Across all datasets, a consistent pattern of least correlation was observed in the equatorial region when compared with NCMRWF analysis data.

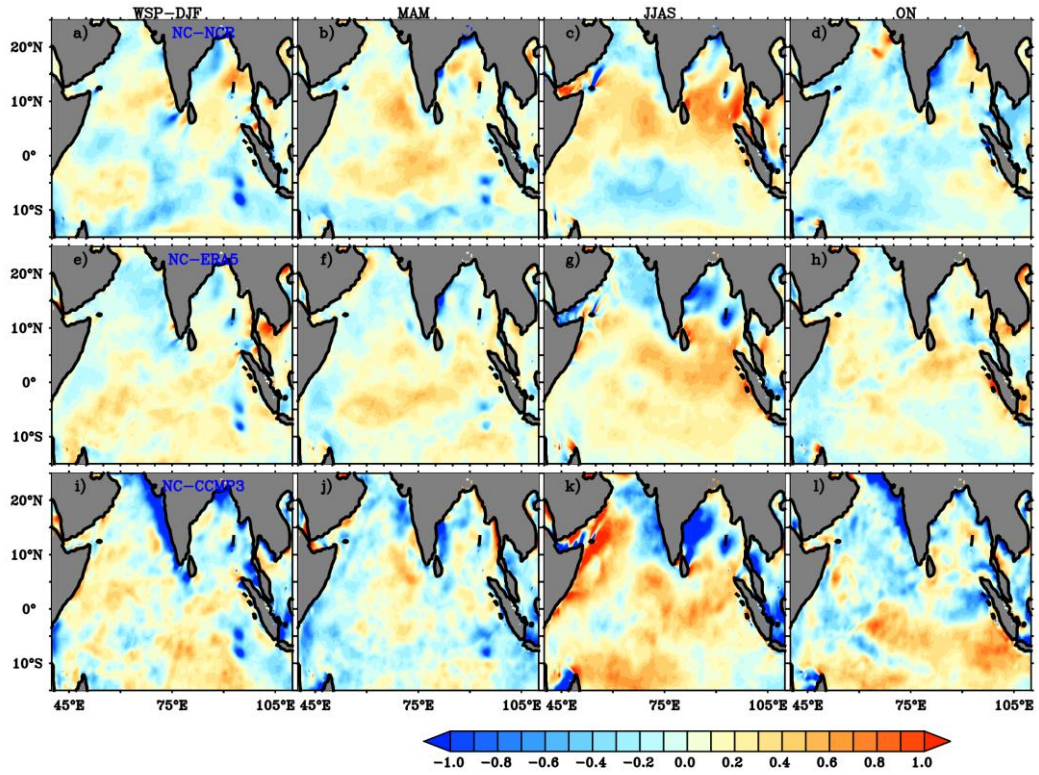


Figure 18: Seasonal wind speed bias of NCMRWF reanalysis (a-d; NCana-NCreana), ERA5 reanalysis (e-h; NCana-ERA5), CCMP3 (i-l;Ncana-CCMP3) with NCMRWF analysis wind speed.

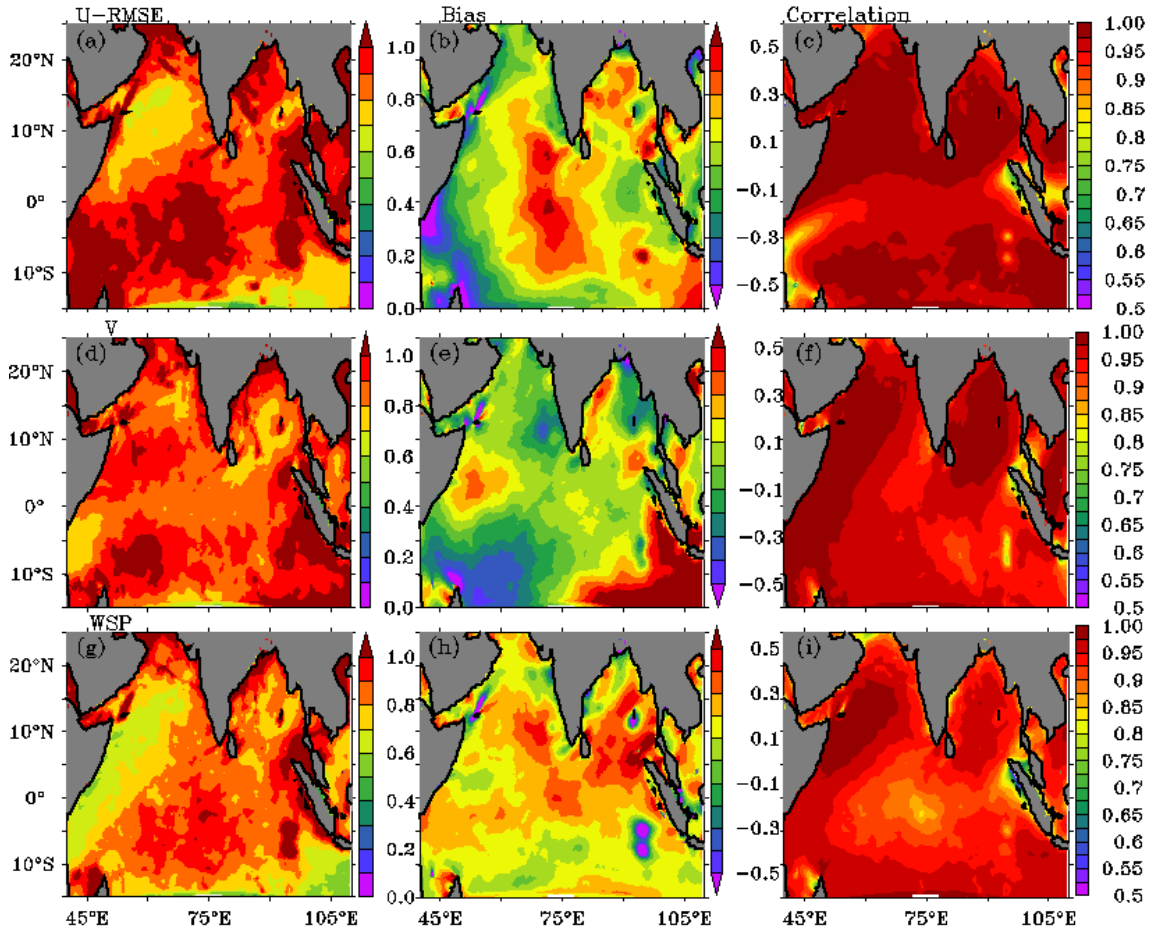


Figure 19: Statistics between NCMRWF-analysis and Re-analysis data (NCAna-NCReana), RMSE(a,d,g), Bias(b,e,h), and Correlation(c,f,i) for zonal, meridional, and wind speed.

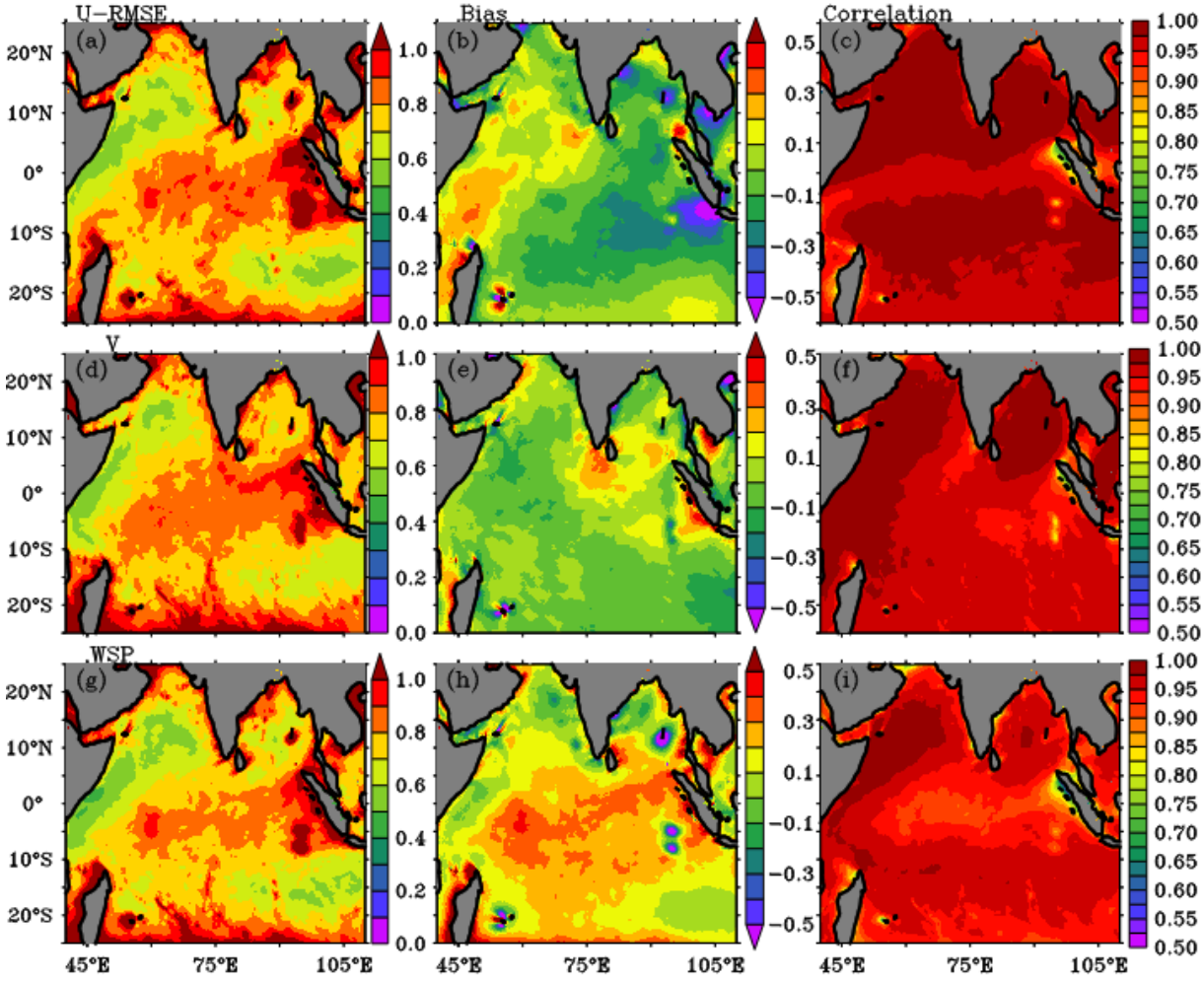


Figure 20: Statistics between NCMRWF-analysis and ERA5 data (NCAna-ERA5), RMSE(a,d,g), Bias(b,e,h), and Correlation(c,f,i) for zonal, meridional, and wind speed.

## 3.3 Validation of Air temperature and Humidity:

### 3.3a Validation of Air temperature:

Wind speed, air temperature, and humidity are crucial parameters for estimating turbulent heat fluxes. These fluxes play a vital role in air-sea interaction processes that occur at the ocean-atmosphere interface and are essential for driving ocean models. Since no satellite observations are available for near-surface air temperature and humidity, these parameters are acquired from atmospheric reanalysis and analysis fields to compute the turbulent fluxes using bulk formula. On the other hand, in-situ observation to compute these fluxes are available but only at few locations. However, these in-situ observations can be used to evaluate the analysis or reanalysis products. Errors in the input parameters for turbulent fluxes can significantly impact the accuracy of the fluxes themselves. Previous studies (Swain et al., 2009, Rahman et al., 2013) have evaluated the importance of wind speed, air temperature, and relative humidity in the estimation of turbulent fluxes. Here, we have evaluated the NCMRWF analysis of air temperature and humidity (RH/SH) with RAMA buoy observations, along with other sources such as NCMRWF reanalysis (IMDAA), ERA5

reanalysis, and OAFlux (an integrated product of blended satellite and analysis data). The locations of the RAMA buoy data used for the present study are detailed in Table 3.

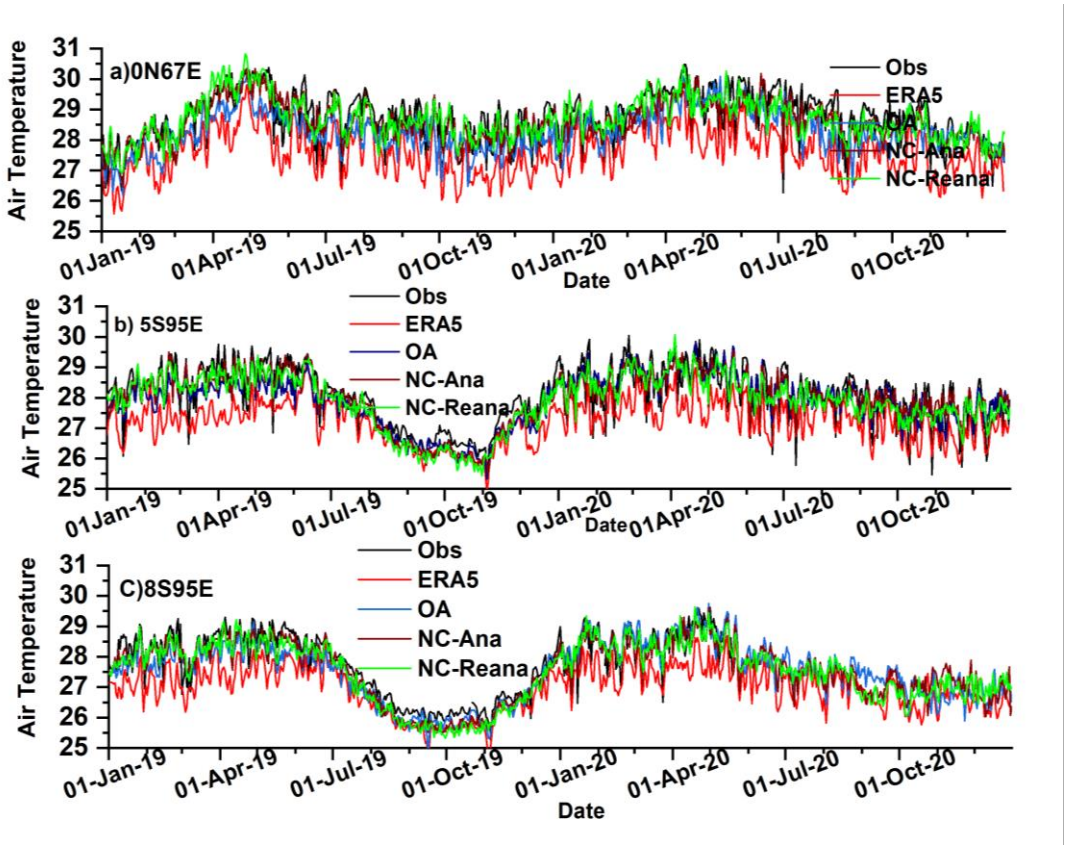


Figure 21:RAMA-Buoy, NCMRWF analysis, NCMRWF reanalysis, ERA5 reanalysis and OAFlux data air temperature (3m) at a)0ºN 67ºE, b)5ºS 95ºE, and c)8ºS 95ºE locations

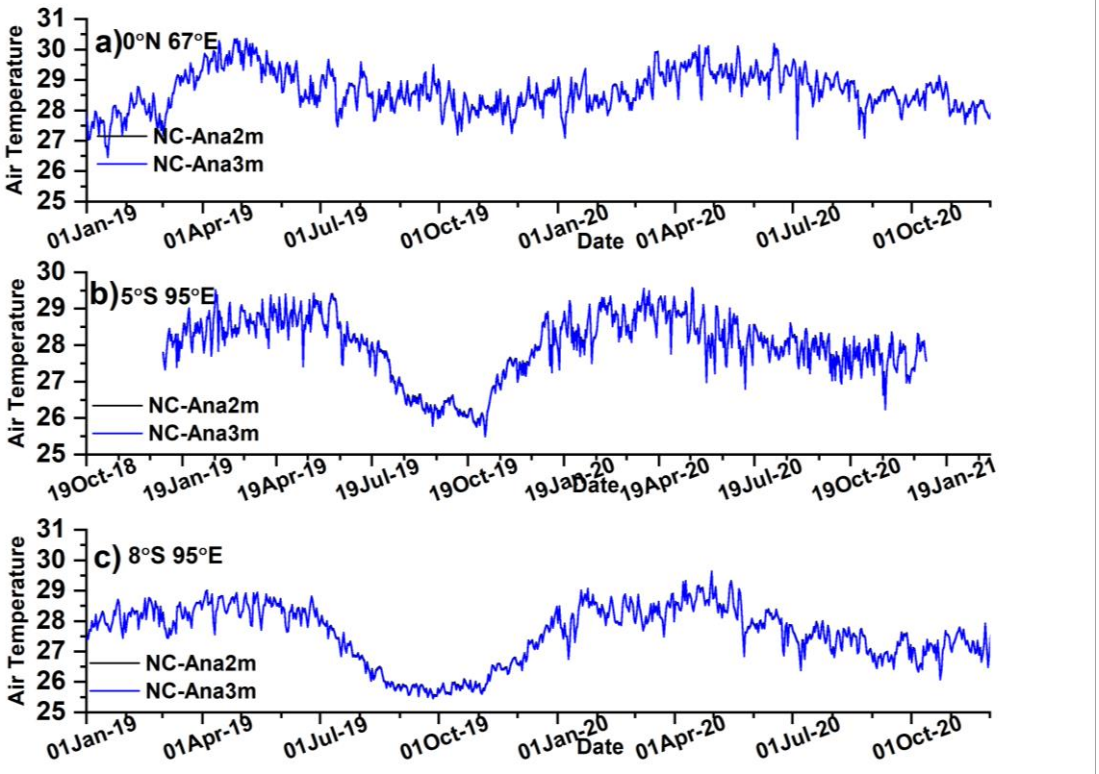


Figure 22: NCMRWF analysis air temperature at 2m and 3m at a)0ºN 67ºE, b)5ºS 95ºE, and c)8ºS 95ºE locations.

The temporal variability of air temperature from in-situ (RAMA buoy) measurements, along with NCMRWF analysis, NCMRWF reanalysis, ERA5 reanalysis, and OAFlux at respective buoy locations, are shown in Figures 21. The time series of air temperature at different buoy locations shows that all products exhibit similar variations with slight deviations from the buoy air temperature. ERA5 air temperature estimates are consistently lower compared to the observed air temperature data from the buoys at their respective locations (Figures 21), with the deviation being minimal from June to December. ERA5 is underestimated largely during wintertime over the southeastern Indian Ocean (Figure 21b). Buoy air temperature is available at a 3m height, while NCMRWF analysis, NCMRWF reanalysis, ERA5 reanalysis, and OA datasets air temperatures are available at 2m. Therefore, the air temperature was corrected from 2m to 3m, and no significant difference was observed in air temperature before and after the height correction, as shown in Figure 22.

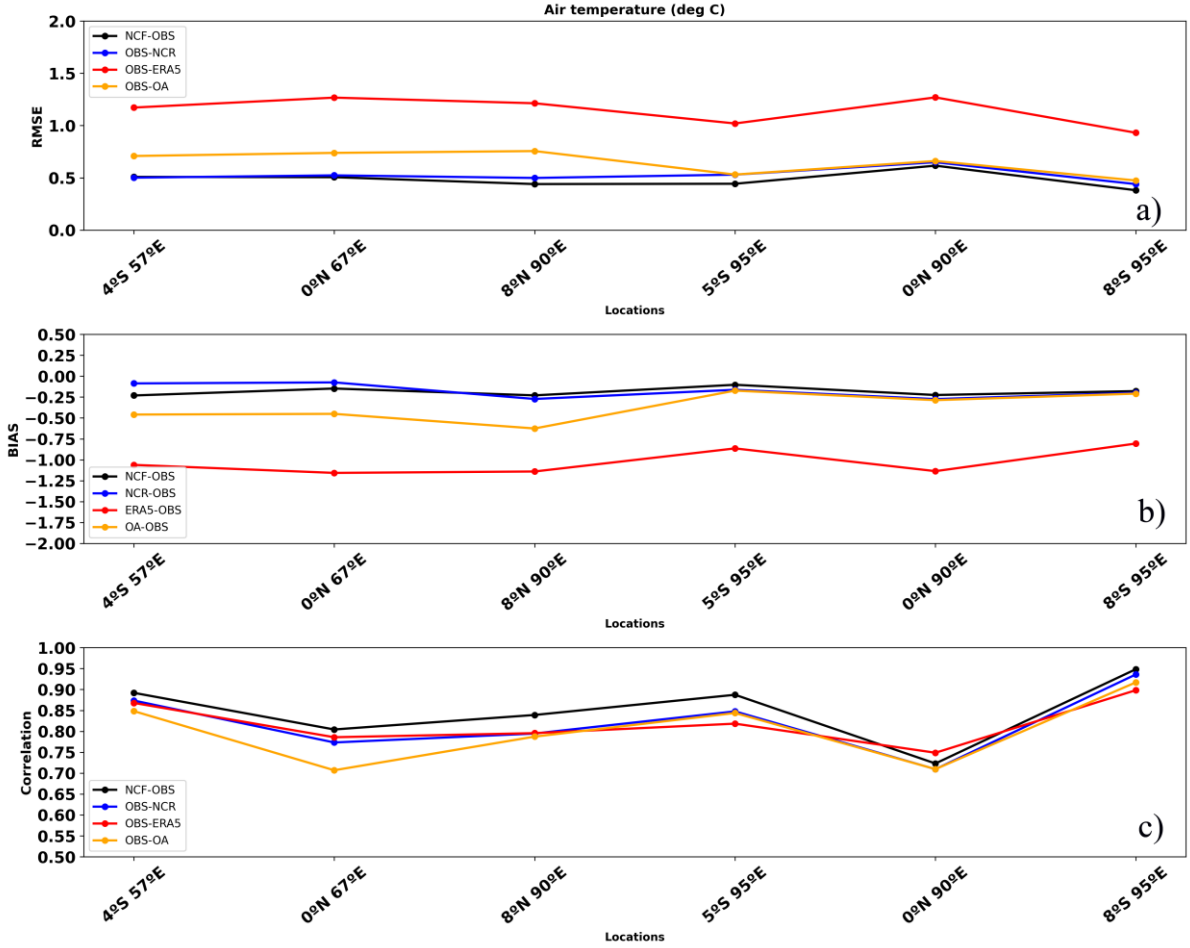


Figure 23: a) RMSE, b) Bias, c) Correlation between RAMA buoy observed air temperature (ºC) and NCMRWF analysis, NCMRWF reanalysis, ERA5 and OAFlux air temperature at respective buoy locations.

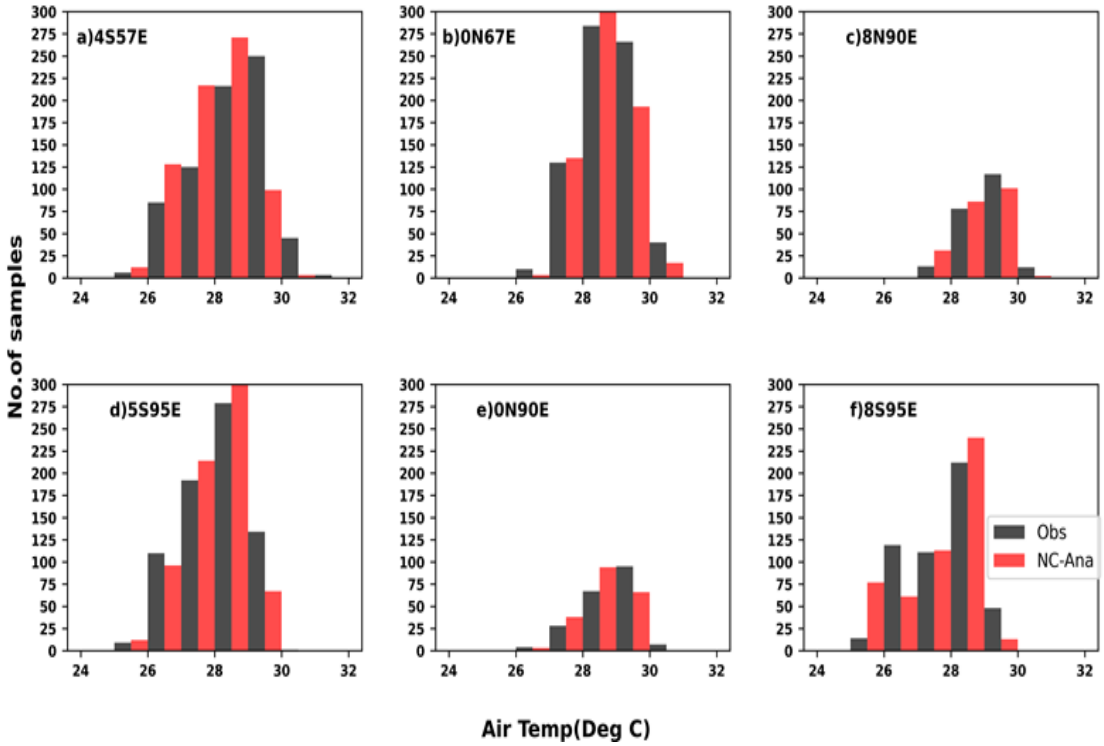


Figure 24: Frequency distribution of RAMA buoy Air temperature (black-bar), and NCMRWF analysis Air temperature (red-bar) over a)4°S 57°E, b)0°N 67°E, c)8°N 90°E, d)5°S 95°E, e)0°N 90°E, f)8°S 95°E locations.

Figure 23 shows the RMSE, BIAS, and CC of air temperature at different buoy locations. The statistical analysis shows that NCMRWF analysis and NCMRWF reanalysis are better correlated with buoy air temperature compared to OAFlux and ERA5 (Table -7). NCMRWF analysis and NCMRWF reanalysis exhibit low RMSE (<0.6 ºC) and low bias (0 to -0.25 ºC), followed by OAFlux (RMSE: 0.5-1 ºC, Bias: 0 to -0.75ºC) and ERA5 (RMSE: 1-1.5 ºC, Bias: -0.75 to -1.25 ºC). All datasets show high correlation at 8 ºS 95 ºE, followed by 4 ºS 57 ºE, 5 ºS 95 ºE, 8 ºN 90 ºE, 0 ºN 67 ºE, and 0 ºN 90 ºE. The NCMRWF analysis air temperature correlation at these locations is 0.95, 0.89, 0.89, 0.84, 0.80, and 0.72 with buoy air temperature, respectively. ERA5, NCMRWF reanalysis, and OAFlux show similar correlations at all buoy locations except at 0ºN 67ºE, as shown in Figure 23c. The frequency distribution indicates that, at almost all locations, in the air temperature range between 27º-29°C, the NCMRWF analysis is higher than buoy observations. However, air temperatures above 29°C are underestimated in the NCMRWF analysis compared to observations (Figure 24). Table 7 shows the statistics between buoy air temperature and NCMRWF analysis, reanalysis, ERA5, and OAFlux air temperature.

Table 7: Statastics between RAMA buoy observed Air temperature, NCMRWF reanalysis, ERA5 reanalysis, and Objectively analyzed flux air temperature (°C). N-number of observations

| | | **Buoy-NCMRWF Analysis** | | | **Buoy-NCMRWF Reanalysis** | | | **Buoy-ERA5 Reanalysis** | | | **Buoy-OAFlux** | | | |
|---|---|---|---|---|---|---|---|---|---|---|---|---|---|---|
| **S.No** | **Location** | **RMSE** | **Cor** | **BIAS-NCF-OBS** | **RMSE** | **Cor** | **BIAS-NCR-OBS** | **RMSE** | **Cor** | **BIAS-ERA-OBS** | **RMSE** | **Cor** | **BIAS-OA-OBS** | **N** |
| 1 | 4°S 57°E | 1.03 | 0.69 | -0.62 | 1.06 | 0.62 | -0.53 | 1.71 | 0.63 | -1.47 | 1.17 | 0.66 | -0.80 | 729 |
| 2 | 0°N 67°E | 0.51 | 0.80 | -0.15 | 0.52 | 0.77 | -0.07 | 1.27 | 0.79 | -1.16 | 0.74 | 0.71 | -0.45 | 729 |
| 3 | 8°N 90°E | 0.44 | 0.84 | -0.23 | 0.50 | 0.79 | -0.27 | 1.21 | 0.80 | -1.14 | 0.76 | 0.79 | -0.63 | 220 |
| 4 | 5°S 95°E | 0.44 | 0.89 | -0.10 | 0.53 | 0.85 | -0.16 | 1.02 | 0.82 | -0.86 | 0.53 | 0.84 | -0.17 | 725 |
| 5 | 8°S 95°E | 0.38 | 0.95 | -0.18 | 0.44 | 0.94 | -0.20 | 0.93 | 0.90 | -0.81 | 0.47 | 0.92 | -0.21 | 504 |
| 6 | 0°N 90°E | 0.62 | 0.72 | -0.23 | 0.65 | 0.71 | -0.27 | 1.27 | 0.75 | -1.14 | 0.66 | 0.71 | -0.29 | 201 |

### 3.3b Spatial variability of Air temperature:

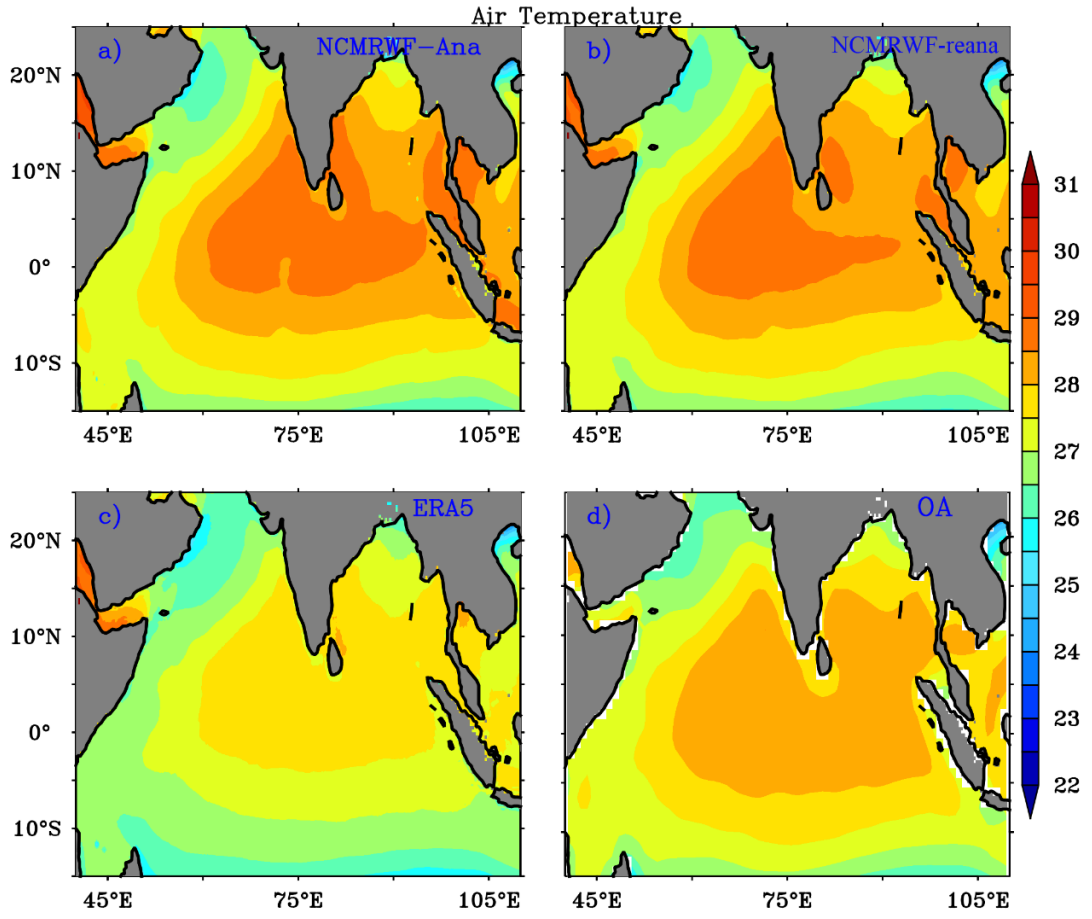


Figure 25: Averaged Air temperature (°C) from 2019-2020: (a) NCMRWF Analysis, (b) NCMRWF Reanalysis, (c) ERA5, and (d) OAFlux.

In the previous section, we found that NCMRWF analysis performed best when compared with buoy observations. Hence, we used NCMRWF analysis to evaluate the spatial distribution of air temperature from other products. The spatial distribution of air temperature from different datasets, such as NCMRWF analysis, NCMRWF reanalysis, ERA5 reanalysis, and OAFlux, over the Indian Ocean for the 2019 and 2020 mean are shown in Figure 25. All datasets show a similar spatial pattern of air temperature. However, ERA5 underestimates by ~ 1° C as compared to other products. This can be seen in the seasonal bias plots (Figure 27 e,f,g,h). NCMRWF analysis and NCMRWF reanalysis exhibit almost the same air temperatures despite having different spatial resolutions. OAFlux shows slightly lower temperatures than NCMRWF analysis, while ERA5 shows the lowest temperatures across all datasets. The seasonal distribution of air temperature is shown in Figure 26. This also shows similar variations in the annual mean.

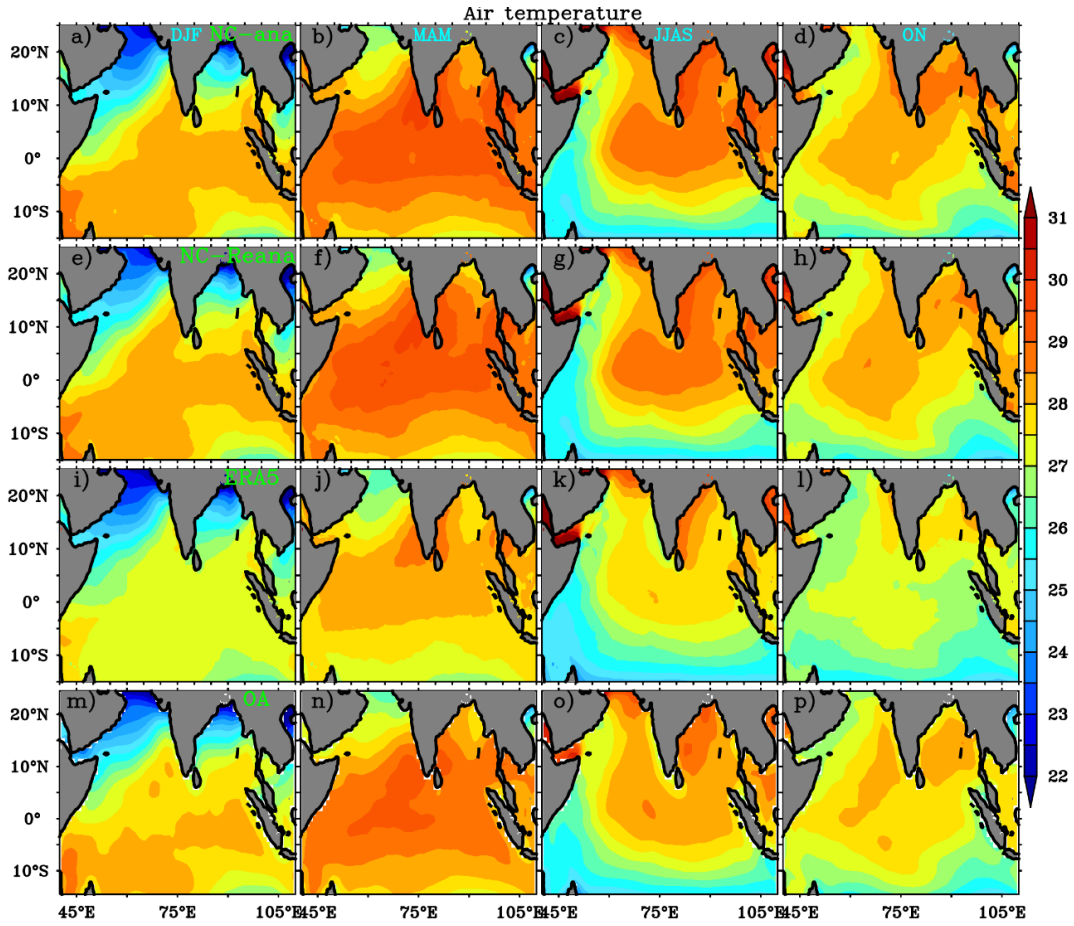


Figure 26: Seasonal averaged Air temperature (°C) (from 2019 to 2020) of NCMRWF analysis (a-d), NCMRWF reanalysis (e-h), ERA5 reanalysis (i-l), and OAFlux (m-p) data.

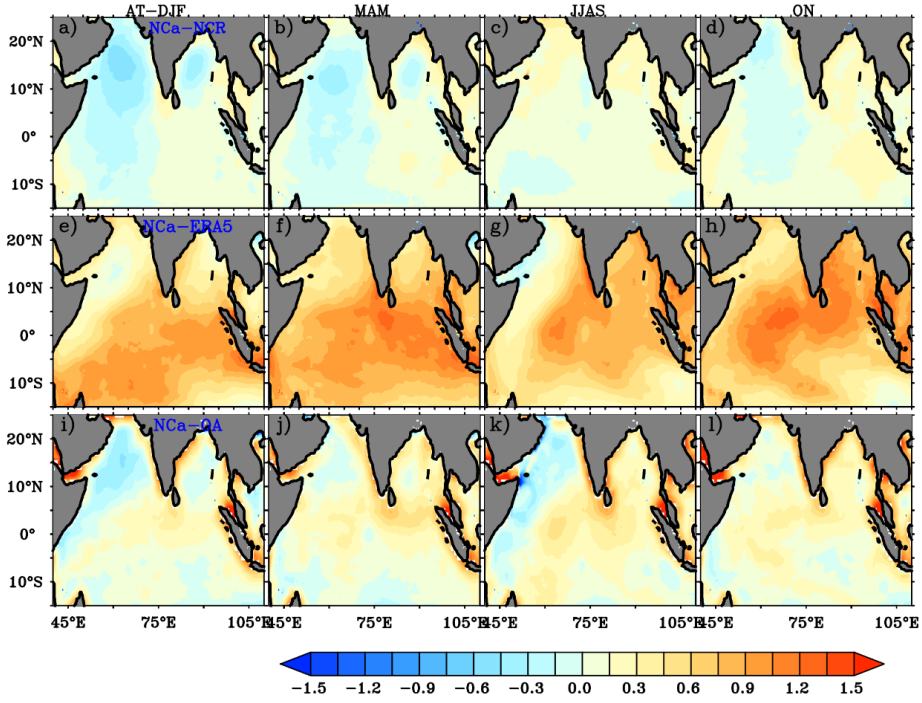


Figure 27: Seasonal Air temperature **(°C)** bias of NCMRWF reanalysis (a-d; NCana-NCreana), ERA5 reanalysis (e-h; NCana-ERA5), OAFlux(i-l;Ncana- OAFlux) with NCMRWF analysis air temperature **(°C)**.

These datasets show higher temperatures over the extensive area of the study region, with peak warming during the pre-monsoon season, followed by the southwest monsoon, and cooling during the northeast monsoon and winter (Figure 26). The lowest air temperatures are observed in ERA5 compared to the remaining datasets. Seasonal bias indicates minimal bias with NCMRWF reanalysis air temperature (-0.3º to 0.3º C) across all seasons, showing a close agreement with the NCMRWF analysis air temperature, followed by OAFlux (bias: -0.6º to 0.6º C) and ERA5 (bias: 1.5º C lower than NCMRWF analysis) (Figure 27).

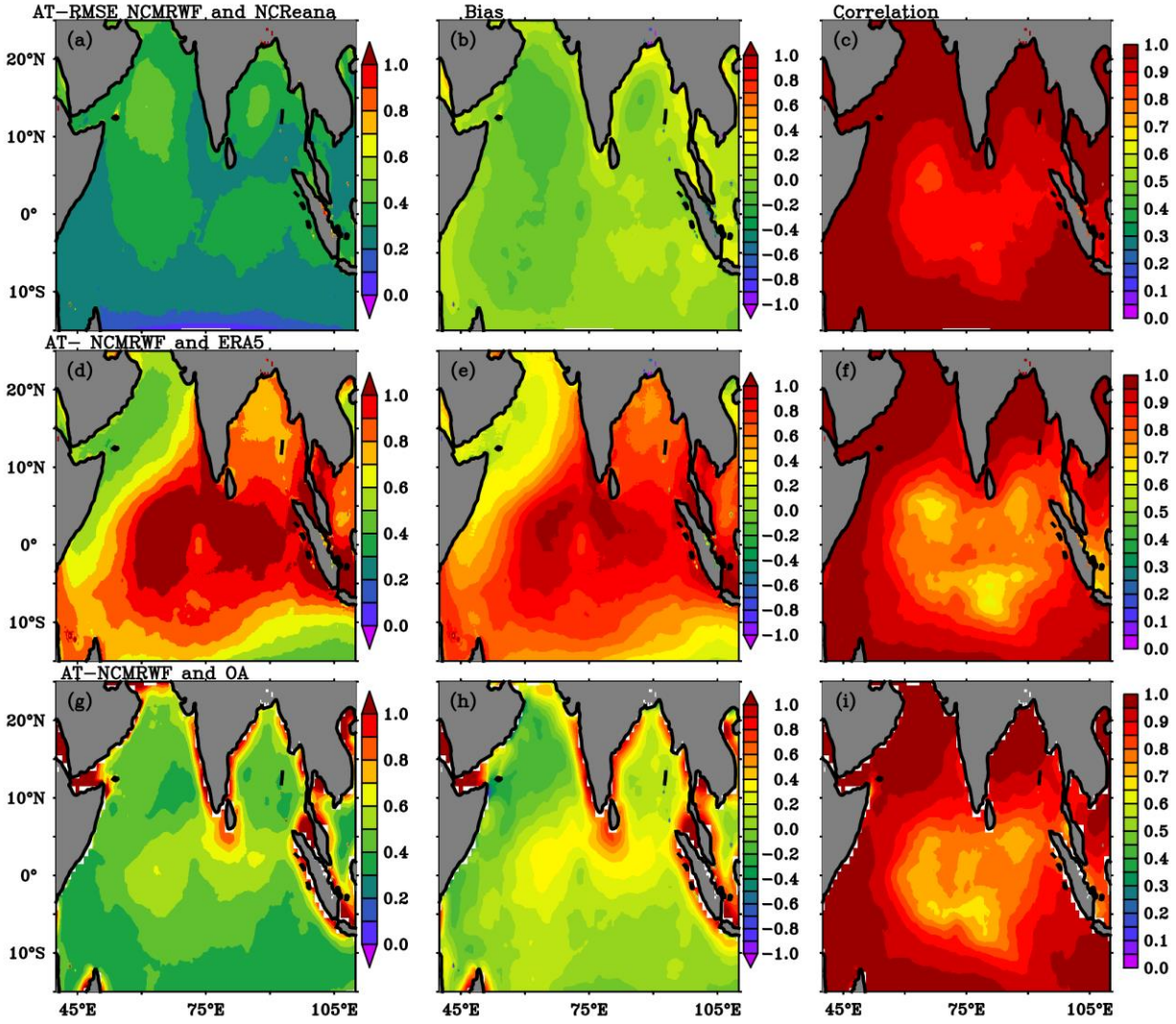


Figure 28: Statistics between NCMRWF analysis and NCMRWF, NCMRWF analysis and ERA5 reanalysis, and NCMRWF analysis and OAFlux. RMSE (a, d, g), Bias (b, e, h), and Correlation (c, f, i) for air temperature (°C)

The statistics collectively illustrate the differences in performance and agreement between NCMRWF analysis, NCMRWF reanalysis, ERA5 reanalysis, and OAFlux datasets (Figure 28). NCMRWF reanalysis air temperature significantly matches with NCMRWF analysis air temperature, with low RMSE (<0.5º C), low bias (-0.3 to 0.3º C), and high

correlation (>0.8) over the study region (Figure 28, lower panel). The NCMRWF reanalysis data and OAFlux show slight deviations from NCMRWF analysis air temperature, with higher RMSE (>0.8º C) and higher bias (>0.5º C) along the coasts, and lower correlation near the equatorial region (0.6-0.8, 10ºN-10ºS). ERA5 air temperature is significantly underestimated compared to NCMRWF analysis, with high RMSE (>0.6º C, excluding the western Arabian Sea), high bias (0.5º C), and low correlation near the equator (0.6-0.8, 10ºN-10ºS). Overall, NCMRWF reanalysis and OAFlux air temperatures match better with NCMRWF analysis air temperature than ERA5 air temperature.

**3.4a Validation of Humidity**:

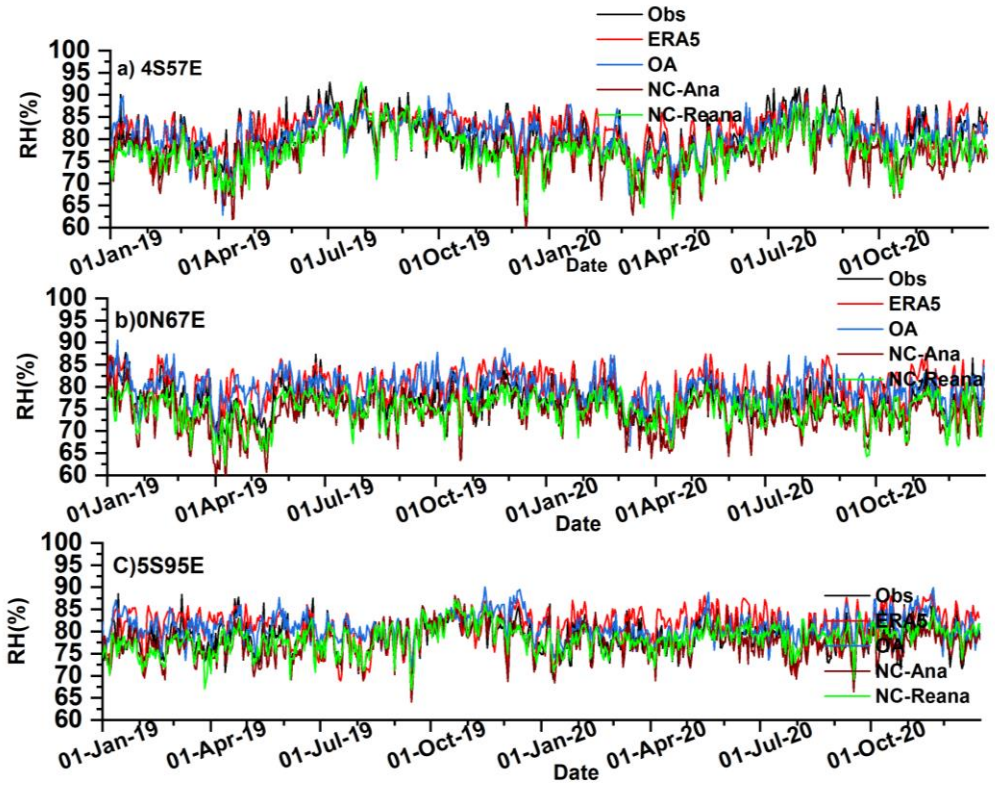


Figure 29: Comparison of Relative Humidity from RAMA buoy, NCMRWF analysis, NCMRWF reanalysis, ERA5 reanalysis, and OAFlux at the following locations: a) 4ºS 67ºE, b) 0ºN 67ºE, and c) 5ºS 95ºE

The time-series of RAMA buoy relative humidity (RH%) along with NCMRWF analysis, NCMRWF reanalysis, ERA5 reanalysis, and OAFlux datasets over the respective buoy locations (listed in Table 7, 8) are shown in Figure 29 (for the locations: 4ºS 67ºE, 0ºN 67ºE, and 5ºS 95ºE). All datasets exhibit similar variability of RH compared to buoy RH with slight deviations. However, Figure 29 clearly illustrates that NCMRWF analysis and reanalysis underestimate RH compared to buoy observations, while ERA5 and OAFlux overestimate RH relative to buoy RH for most of 2019 and 2020. The reanalysis and satellite datasets provide the specific humidity at 2m. The height was corrected to 3m, and RH was

computed from the specific humidity. Hence, the NCMRWF analysis-specific humidity at 2m and 3m (corrected from 2m to 3m to match the buoy observations at 3m) displays no significant difference before and after the height correction(Figure 30).

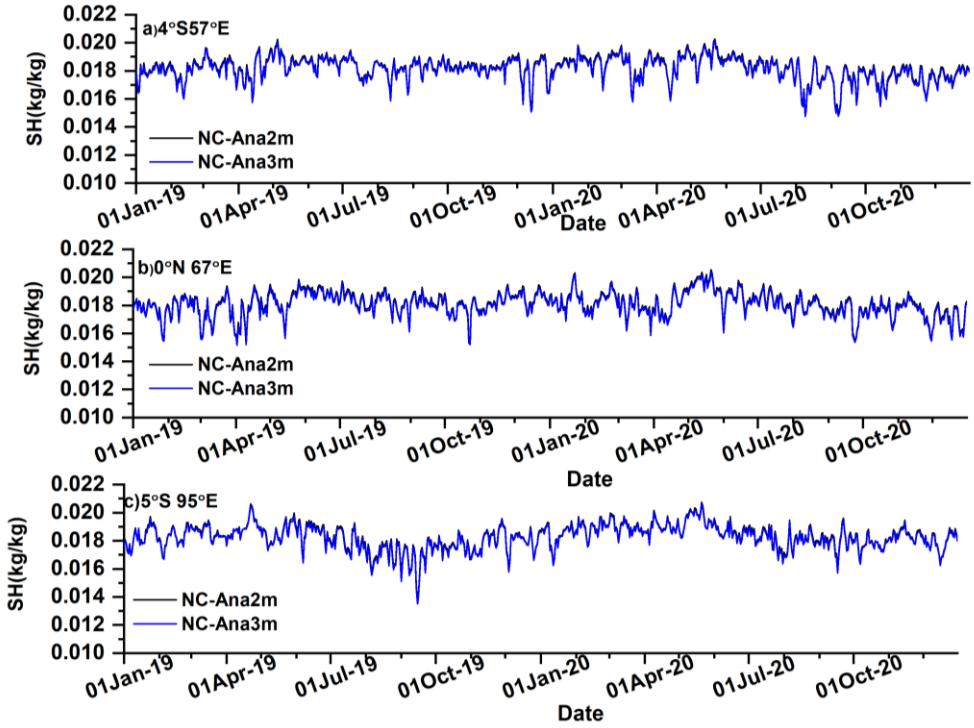


Figure 30: NCMRWF analysis specific humidity at 2m and 3m at a) 4ºS 67ºE, b) 0ºN 67ºE, and c) 5ºS 95ºE

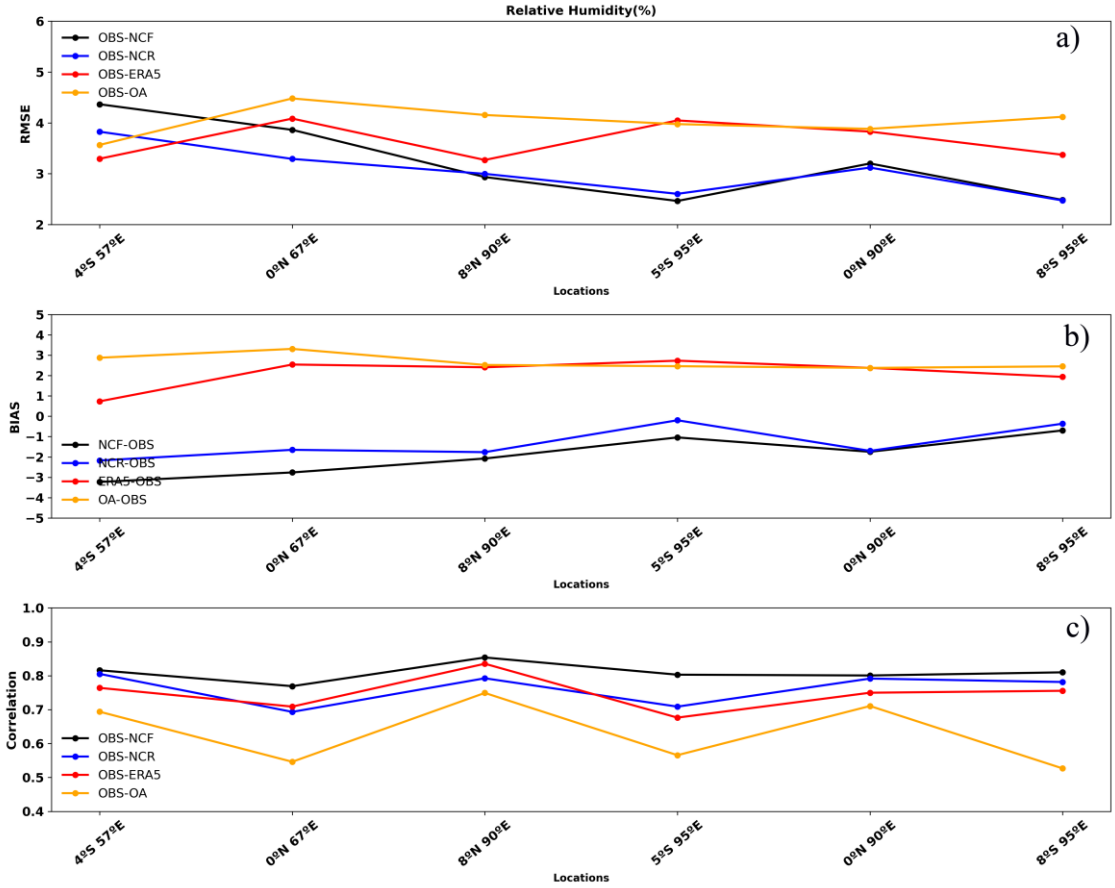


Figure 31: a)RMSE, b)Bias, c)Correlation between RAMA buoy observed Relative humidity (%) and NCMRWF analysis, NCMRWF reanalysis, ERA5 and OAFlux Relative humidity at respective buoy locations.

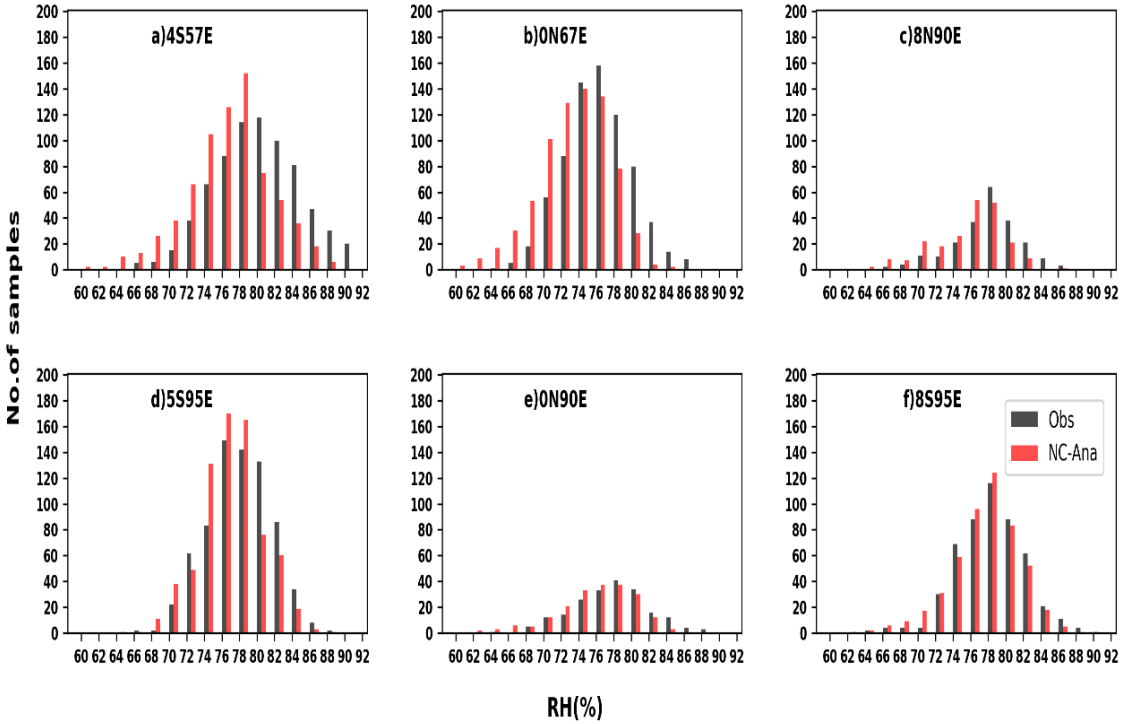


Figure 32: Frequency distribution of RAMA buoy Relative Humidity (black-bar), and NCMRWF analysis Relative Humidity (red-bar) over a)4°S 57°E, b)0°N 67°E, c)8°N 90°E, d)5°S 95°E, e)0°N 90°E, f)8°S 95°E locations.

The NCMRWF analysis and reanalysis show the lowest RMSE and bias (underestimated than observation), as well as a high correlation with observations. ERA5 also performs well, although it shows higher bias (overestimated than observation) even compared to the NCMRWF datasets, except at 4°S 57°E. The OAFlux data tend to have higher RMSE and bias (overestimated than observation) values when compared with observed buoy relative humidity. The correlation analysis shows that the NCMRWF analysis has the highest correlation with buoy relative humidity, while the OAFlux data exhibit the least correlation at all locations (Table 8, Figure 31).

The frequency distribution (Figure 32) of NCMRWF analysis and observed buoy RH shows that the NCMRWF analysis is overestimating the buoy-observed RH at 4°S 57°E, 5°S 95°E, and 8°S 95°E for RH <78%. However, at 8°N 90°E and 0°N 90°E, the NCMRWF analysis RH is overestimated when RH is <76%, and at 0°N 67 °E, when RH is <72%.

Table 8: Statastics between RAMA buoy observed Relative humidity, NCMRWF reanalysis, ERA5 reanalysis, and Objectively analyzed flux Relative Humidity (%). N-number of observations

| | | Buoy-NCMRWF Analysis | | | Buoy-NCMRWF Reanalysis | | | Buoy-ERA5 Reanalysis | | | Buoy-OAFlux | | | |
|---|---|---|---|---|---|---|---|---|---|---|---|---|---|---|
| **S.No** | **Location** | **RMSE** | **Cor** | **BIAS-NCF-OBS** | **RMSE** | **Cor** | **BIAS-NCR-OBS** | **RMSE** | **Cor** | **BIAS-ERA-OBS** | **RMSE** | **Cor** | **BIAS-OA-OBS** | **N** |
| 1 | 4°S 57°E | 4.37 | 0.82 | -3.23 | 3.83 | 0.81 | -2.17 | 3.29 | 0.76 | 0.73 | 3.57 | 0.69 | 2.88 | 729 |
| 2 | 0°N 67°E | 3.86 | 0.77 | -2.76 | 3.29 | 0.69 | -1.65 | 4.08 | 0.71 | 2.54 | 4.48 | 0.55 | 3.31 | 729 |
| 3 | 8°N 90°E | 2.93 | 0.85 | -2.08 | 3.00 | 0.79 | -1.77 | 3.27 | 0.84 | 2.41 | 4.15 | 0.75 | 2.52 | 220 |
| 4 | 5°S 95°E | 2.46 | 0.80 | -1.04 | 2.60 | 0.71 | -0.20 | 4.05 | 0.68 | 2.73 | 3.98 | 0.57 | 2.46 | 725 |
| 5 | 8°S 95°E | 2.48 | 0.81 | -0.70 | 2.47 | 0.78 | -0.37 | 3.37 | 0.76 | 1.93 | 4.12 | 0.53 | 2.45 | 504 |
| 6 | 0°N 90°E | 3.20 | 0.80 | -1.75 | 3.12 | 0.79 | -1.70 | 3.83 | 0.75 | 2.38 | 3.88 | 0.71 | 2.38 | 201 |

### 3.4b Spatial variability of Specific Humidity (Qa):

Similar to air temperature for Specific Humidity too, NCMRWF analysis performs best among all when compared with buoy observations. Hence, NCMRWF analysis specific humidity was used to evaluate other products for spatial variation. The spatial distribution of two years mean (from 2019 to 2020) specific humidity (Qa, in g/kg) from the NCMRWF analysis, reanalysis, ERA5, and OAFlux are shown in Figure 33. The spatial distribution of Qa indicates that all datasets show similar distribution and variability. OAFlux is the highest estimated, and ERA5 is the lowest estimated specific humidity compared to the NCMRWF analysis.

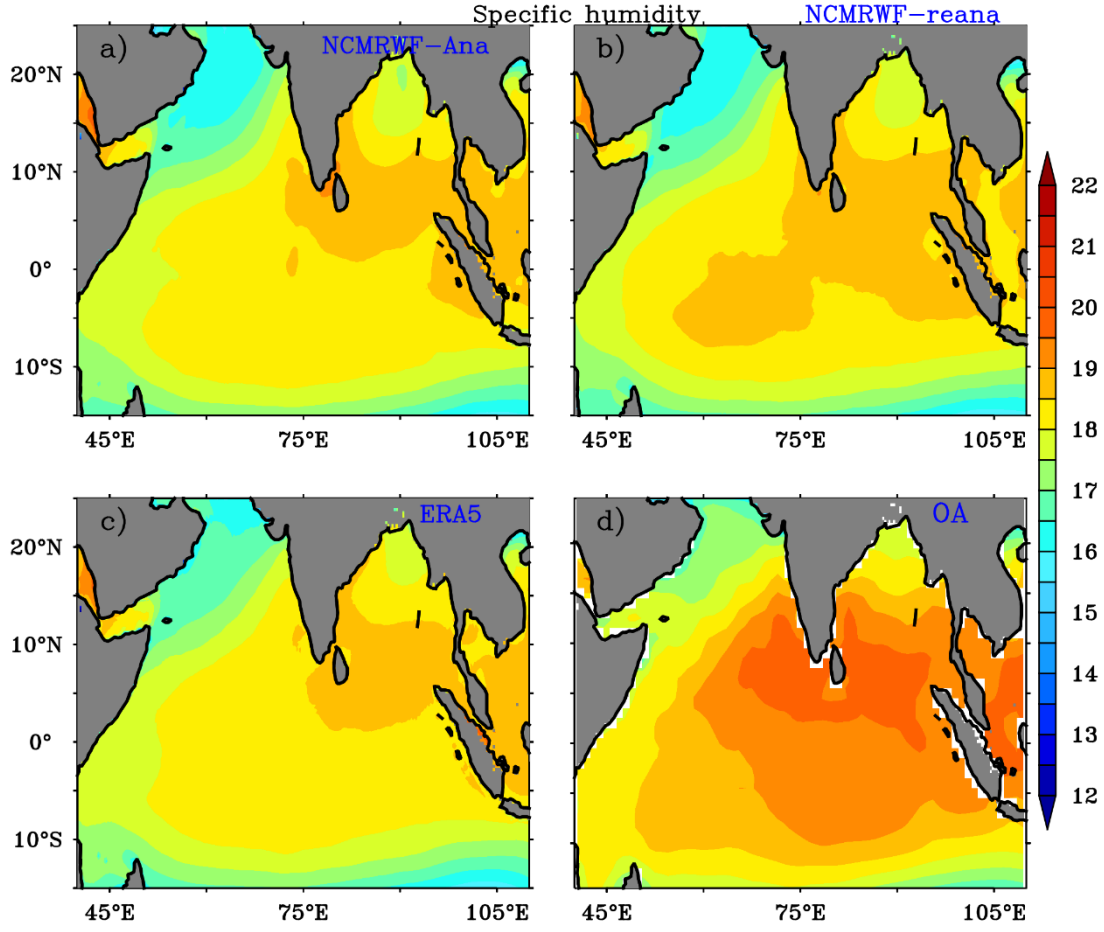


Figure 33: Annual averaged Specific humidity **($Q_a$) (2019-2020):** (a) NCMRWF Analysis, (b) NCMRWF Reanalysis, (c) ERA5, and (d) OAFlux.

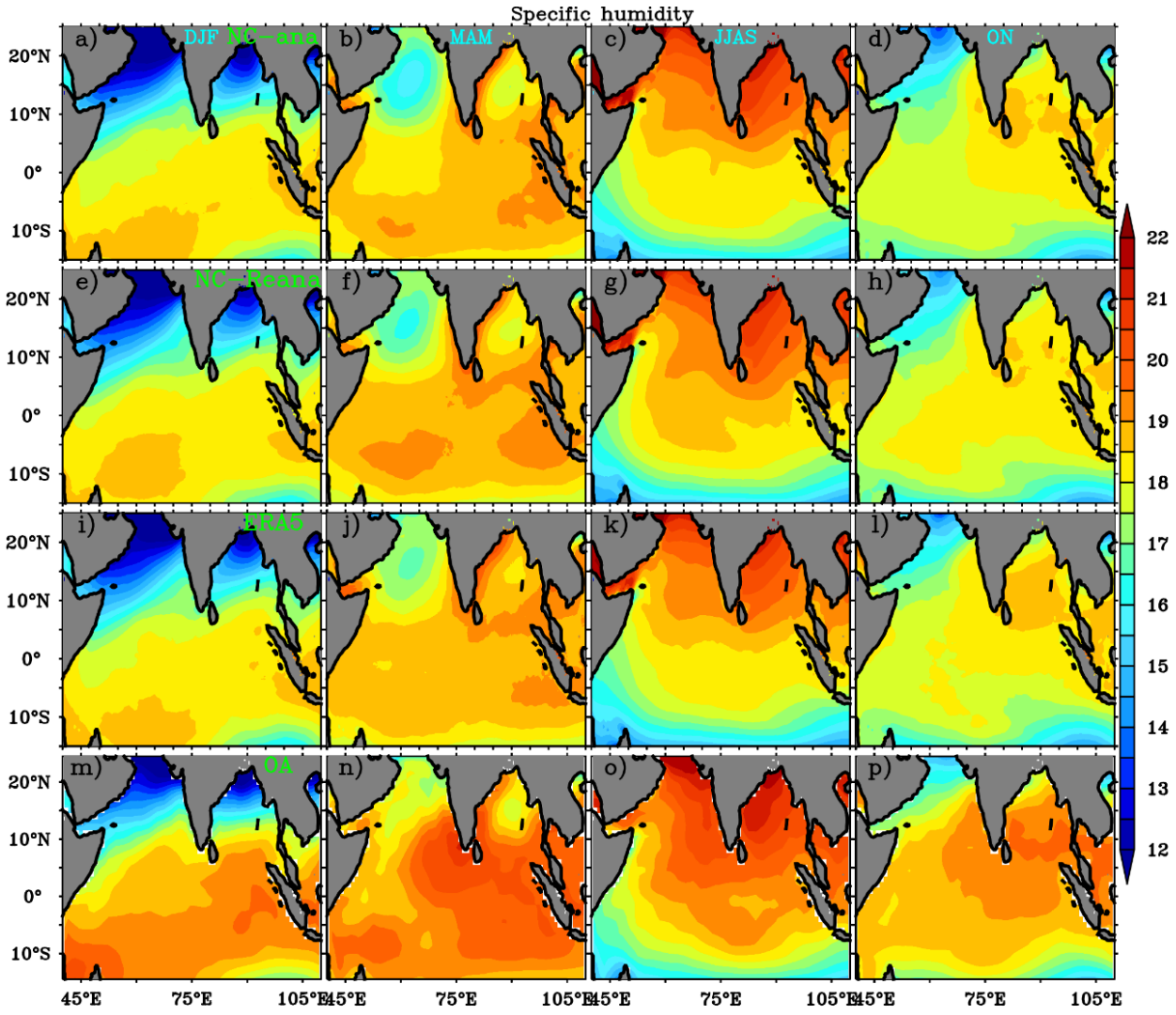


Figure 34: Seasonal averaged Specific humidity ($Q_a$) (from 2019 to 2020) of NCMRWF analysis (a-d), NCMRWF reanalysis (e-h), ERA5 reanalysis (i-l), and OAFlux (m-p) data.

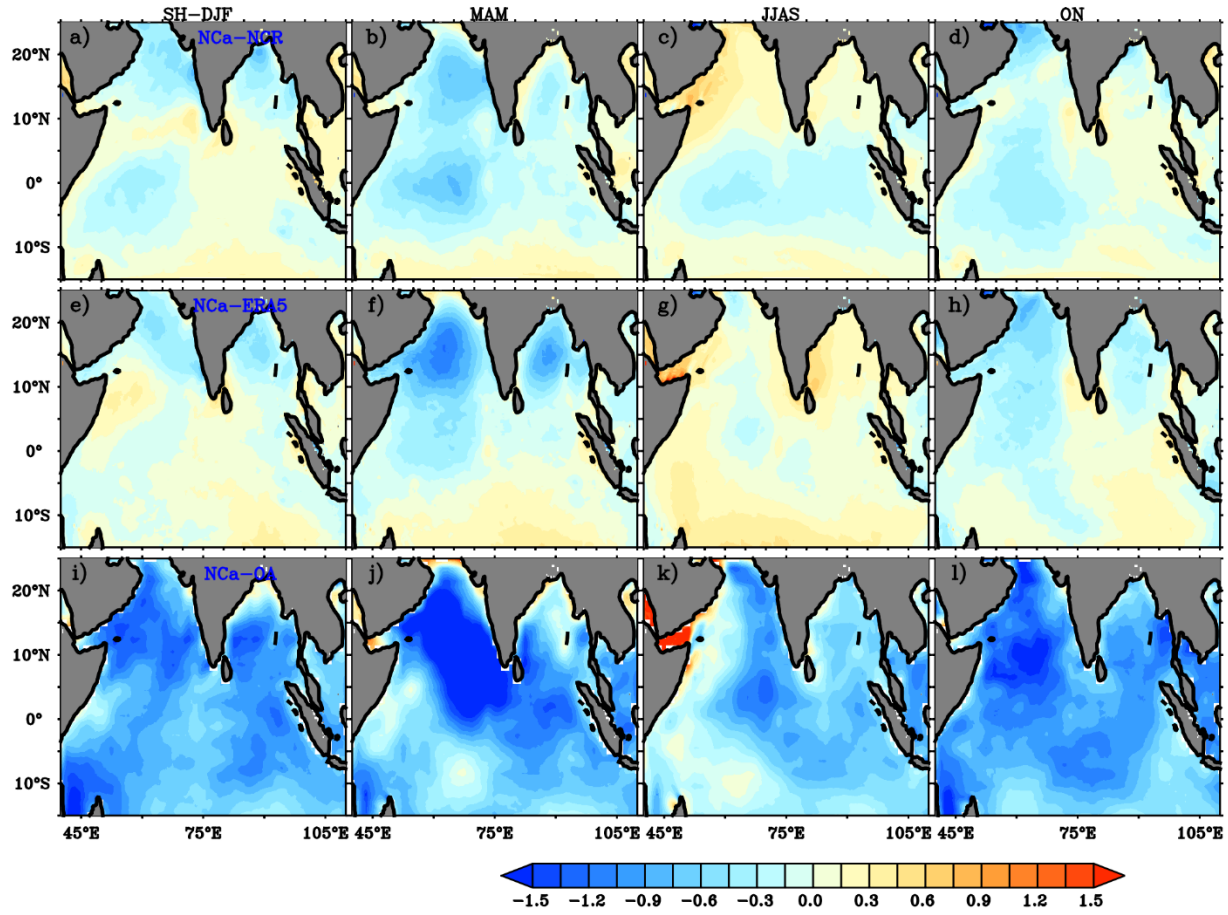


Figure 35: Seasonal Specific humidity (Qa) bias of NCMRWF reanalysis (a-d; NCana-NCreana), ERA5 reanalysis (e-h; NCana-ERA5), OAFlux (i-l;Ncana- OAFlux) with NCMRWF analysis Specific humidity (Qa).

Comparing Qa across different datasets, OAFlux shows the highest Qa among all datasets in all seasons. The Qa distribution and variability in NCMRWF reanalysis and OAFlux are significantly aligned with the NCMRWF analysis Qa, with OAFlux showing slightly higher variability and higher values (~1 g/kg) than the NCMRWF analysis Qa (Figure 34), especially in the Arabian Sea and south of the equator. Seasonal bias (Figure 35) clearly illustrates that NCMRWF reanalysis and ERA5 show less bias (-0.5 to 0.5 g/kg), and both datasets overestimate Qa over the Arabian Sea in winter, pre-monsoon and northeast monsoon seasons. OAFlux consistently overestimates Qa across the large areas of the study region in all seasons by more than -0.5 g/kg, with the highest bias in the Arabian Sea during the pre-monsoon season and the least in the monsoon season (Figure 35).

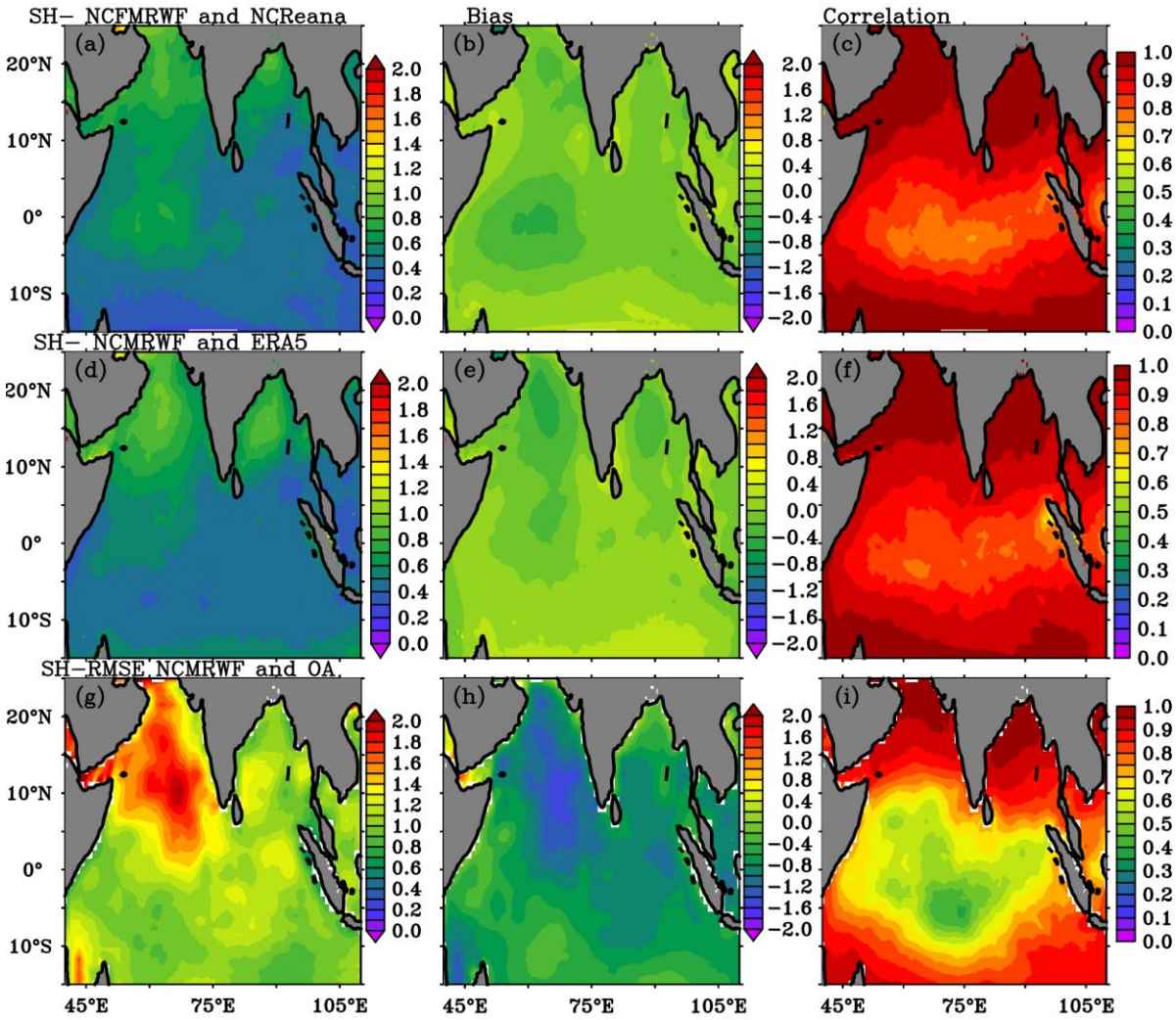


Figure 36: Statistics between NCMRWF analysis and NCMRWF, NCMRWF analysis and ERA5 reanalysis, and NCMRWF analysis and OAFlux. RMSE (a, d, g), Bias (b, e, h), and Correlation (c, f, i) for Specific Humidity.

The statistics between the NCMRWF analysis and NCMRWF reanalysis, ERA5, and OAFlux are illustrated in Figure 36, showing RMSE (a, d, g), bias (b, e, h), and correlation (c, f, i). OAFlux exhibits high RMSE and bias (OA Qa is higher than NCMRWF analysis Qa), particularly in the Arabian Sea (>1 g/kg), and lower correlation (0.4 to 0.7) between 10°N and 10°S. Similar patterns, with lower RMSE and bias, are observed in the NCMRWF reanalysis and ERA5 compared to the NCMRWF analysis Qa. However, the lowest correlation (0.7) is observed between 10°N and 10°S. All datasets show a good correlation (more than 0.9) in the northern Indian Ocean.

## 4. Summary and Conclusion:

The Indian summer monsoon is crucial for the country in various aspects, including agriculture, water resources, and economic stability. Hence, reliable monsoon forecasts are essential. INCOIS provides near real-time global analysis with the Global Ocean Data Assimilation System (GODAS), which was adopted from NOAA/NCEP in 2013. This

analysis is used for the crucial initial conditions for the CFSv2 coupled model, which was used for the seasonal Indian Summer Monsoon Rainfall (ISMR) forecast. Accurate ocean initialization is required for better ISMR seasonal prediction. GODAS analysis was produced using the forcing fields from NCMRWF GFS atmospheric analysis. Bulk-algorithm is used to compute turbulent heat and momentum fluxes using the near-surface NCMRWF analysis fields. Studies show that errors in the input fields, particularly near-surface wind, air temperature, and humidity, significantly affect the heat and momentum flux computation using a bulk algorithm. Hence, we evaluate the performance of NCMRWF near-surface atmospheric fields, for 2019 and 2020 using RAMA buoy observations. We also evaluated NCMRWF reanalysis, ERA5 reanalysis, and CCMP3-satellite-derived surface wind fields and the near-surface AT and RH. This evaluation was conducted quantitatively using several statistical measures. The statistical errors were estimated using the two years of collocated data for NCMRWF and buoy surface zonal (u) and meridional (v) wind components, air temperature, and specific humidity.

Since observed RAMA buoy winds are available at a 4m height and other datasets provide winds at a 10m height, an algorithmic method was used to correct the wind height from 10m to 4m. We then performed error statistics (mean, bias, RMSE, standard deviation, and correlation), which revealed that the NCMRWF analysis matched well with observed buoy winds at all locations, followed by NCMRWF reanalysis, ERA5 reanalysis, and CCMP3. However, high RMSE, bias, and low correlation were noted in the southeast equatorial region for the NCMRWF analysis fields. CCMP3 has shown high RMSE and low correlation at all locations with buoy winds. The zonal and meridional wind frequency distribution diagrams indicate that NCMRWF analysis overestimates the low wind regime (-2 to 2 m/s) compared to observed winds at 95°E 5°S and 95°E 8°S. The same results were also found for the low wind speeds of less than 2 m/s. NCMRWF analysis winds correlate better with observed winds than NCMRWF reanalysis, ERA5 reanalysis, and CCMP3 winds. The spatial distribution of wind fields shows similar patterns for all products. However, ERA5 reanalysis underestimates other fields by ~ 0.5-1 m/s. Overall, NCMRWF wind performs best among all, and satellite-derived wind CCMP performs poorest when compared with buoy observations.

NCMRWF analysis, NCMRWF reanalysis, ERA5, and OAFlux air temperature and specific humidity are available at a 2 m height, while RAMA buoy relative humidity is available at a 3m height. Therefore, all air temperatures and specific humidity were corrected to a 3m height for comparison (relative humidity computed from specific humidity at 3 m). Time series analysis shows all the products are able to capture the daily observed AT variations. However, all products underestimate the air temperature compared to buoy-

observed air temperature. ERA5 air temperature is lower than the observed air temperature and even lower than NCMRWF analysis, reanalysis, and OAFlux air temperatures. The frequency distribution shows that, at almost all locations, the NCMRWF analysis is higher than buoy observations in the air temperature range between 27-29°C. The overall statistics show RMSE values are the least in NCMRWF analysis ( ~ 0.5 C) and highest in ERA5 ( ~ 1 m/s) (Table -7). The spatial distribution and variability of the NCMRWF analysis, NCMRWF reanalysis, ERA5 reanalysis, and OAFLUX air temperature show the same pattern, with ERA5 estimating lower air temperatures compared to all other products.

Similar to AT, RH also could able to capture the observed daily variability. However, the NCMRWF analysis and NCMRWF reanalysis underestimate relative humidity compared to buoy-observed relative humidity, while ERA5 and OAFlux overestimate it. Among all datasets, the NCMRWF analysis shows the highest correlation with buoy relative humidity, followed by NCMRWF reanalysis, ERA5, and OAFlux. The frequency distribution of NCMRWF analysis and buoy-observed relative humidity shows that the NCMRWF analysis overestimates the buoy-observed relative humidity at 4°S 57°E, 5°S 95°E, and 8°S 95°E for relative humidity <78%. However, at 8°N 90°E and 0°N 90°E, the NCMRWF analysis overestimates relative humidity when it is <76%, and at 0°N 67 °E, when it is <72%.

The specific humidity from NCMRWF analysis is compared with NCMRWF reanalysis, ERA5, and OAFlux. Spatial distribution and time series analysis show that OAFlux tends to overestimate specific humidity compared to all other datasets. The NCMRWF analysis data performs best among all other products when compared with buoy observations. The RMSE values are higher in OAFlux and ERA5 ( ~ 4 %), but it's less in NCMRWF analysis and reanalysis ( ~ 3 %) products with the least values in NCMRWF analysis. Biases are also of similar order (Table 8). This analysis shows that among all products, NCMRWF analysis fields perform best among all. With respect to NCMRWF and ERA5 reanalysis, NCMRWF outperformed.

## 5. Reference:

Dora, G. U., Kankara, R. S., & Rasheed, K. (2019). Evaluation of the reanalysis wind over the Indian Ocean across the seasonal reversing wind pattern.Indian journal of Geo-Marine sciences. Vol. 48 (01), January 2019, pp. 75-84

Goswami, B.N., Rajagopal, E.N. Indian Ocean surface winds from NCMRWF analysis as compared to QuikSCAT and moored buoy winds. *J Earth Syst Sci* **112**, 61–77 (2003). https://doi.org/10.1007/BF02710044

Hersbach, H., Bell, B., Berrisford, P., Biavati, G., Horányi, A., Muñoz Sabater, J., Nicolas, J., Peubey, C., Radu, R., Rozum, I., Schepers, D., Simmons, A., Soci, C., Dee, D., Thépaut, J-N. (2023): ERA5 hourly data on single levels from 1940 to present. Copernicus Climate Change Service (C3S) Climate Data Store (CDS), DOI: 10.24381/cds.adbb2d47

John P George, S. Indira Rani, A. Jayakumar, Saji Mohandas, Swapan Mallick, R. Rakhi, M. N. R.Sreevathsa and E. N. Rajagopal (2016). NCUM Data Assimilation System, NMRF/TR/01/2016,20p. (https://www.ncmrwf.gov.in/NCUM-Data%20Assimilation.pdf).

Kameshwari, N., Bhaskar, T. U., Rao, E. P. R., & Jampana, V. (2022). Enhanced marine meteorological atlas for tropical Indian Ocean. *Journal of Earth System Science*, *131*(2), 107.

Large W G and Pond S 1981 Open ocean momentum Cux measurements in moderate to strong winds; J. Phys.Oceanogr. 11(3) 324–336.

Large, W. G., & Pond, S. (1982). Sensible and latent heat flux measurements over the ocean. *Journal of physical Oceanography*, *12*(5), 464-482.

McPhaden, M. J., Ando, K., Bourles, B., Freitag, H. P., Lumpkin, R., Masumoto, Y., Yu, W. (2010). The global tropical moored buoy array. *Proceedings of OceanObs*, *9*, 668-682.

Mears, Carl., Lee, T., Ricciardulli, L., Wang, X., & Wentz, F. (2022). Improving the accuracy of the cross-calibrated multi-platform (CCMP) ocean vector winds. *Remote Sensing*, *14*(17), 4230.

Modi, A., Munaka, S. K., Harikumar, R., Nair, T. B., & Srinivas, K. (2021). Evaluation of winds from SCATSAT-1 and ASCAT using buoys in the Indian Ocean. *Journal of the Indian Society of Remote Sensing*, *49*, 1915-1925.

Peixoto, J. P., & Oort, A. H. (1992). Physics of Climate. American Institute of Physics, New york.

Prasad, V. S., C. J. Johny, P. Mali, Sanjeev Kumar Singh, and E. N. Rajagopal. (2016). “Retrospective Analysis of NGFS for the years 2000-2011”. Current Science, vol,112,No2,370-377

Rahaman, H., and M. Ravichandran (2013), Evaluation of near-surface air temperature and specific humidity from hybrid global products and their impact on latent heat flux in the North Indian Ocean, J. Geophys. Res. Oceans, 118, 1034–1047, doi:10.1002/jgrc.20085.

Rani, S. I., Arulalan, T., George, J. P., Rajagopal, E. N., Renshaw, R., Maycock, A., ... & Rajeevan, M. (2021). IMDAA: High-resolution satellite-era reanalysis for the Indian monsoon region. *Journal of Climate*, *34*(12), 5109-5133.

Rani, S.I., John P. George, T. Arulalan, Sumit Kumar, M. Das Gupta, E.N. Rajagopal and Richard Renshaw (2020), "Evaluation of High Resolution IMDAA Regional Reanalysis Precipitation over India during Summer Monsoon Season", CLIVAR Exchanges - Special Issue: India's Monsoon Mission, No.79, Pages 31-33, November 2020 DOI: https://doi.org/10.36071/clivar.79.2020.

Rawlins, F., Ballard, S. P., Bovis, K. J., Clayton, A. M., Li, D., Inverarity, G. W., ... & Payne, T. J. (2007). The Met Office global four-dimensional variational data assimilation scheme. *Quarterly Journal of the Royal Meteorological Society: A journal of the atmospheric sciences, applied meteorology and physical oceanography*, *133*(623), 347-362.

Sanjib K. Deb , Suchandra A. Bhowmick , Raj Kumar & Abhijit Sarkar (2009).Inter-Comparison of Numerical Model Generated Surface Winds with QuikSCAT Winds over the Indian Ocean, Marine Geodesy, 32:4, 391-408, DOI: 10.1080/01490410903297865

Sumit Kumar, A. Jayakumar, M. T. Bushair, Buddhi Prakash J., Gibies George, Abhishek Lodh, S. Indira Rani, Saji Mohandas, John P. George and E. N. Rajagopal. (2018). Implementation of New High Resolution NCUM Analysis-Forecast System in Mihir HPCS, NMRF/TR/01/2018, 17p. (https://www.ncmrwf.gov.in/NCUM-Report-Aug2018_final.pdf)

Sumit Kumar, M. T. Bushair, Buddhi Prakash J., Abhishek Lodh, Priti Sharma, Gibies George, S. Indira Rani, John P. George, A. Jayakumar, Saji Mohandas, Sushant Kumar, Kuldeep Sharma, S. Karunasagar and E. N. Rajagopal. (2020). NCUM Global NWP System: Version 6 (NCUM-G:V6),NMRF/TR/06/2020, 32p. (https://www.ncmrwf.gov.in/New_NCUM- Implementation_Report)

Swain, D., Rahman, S. H., & Ravichandran, M. (2009). Comparison of NCEP turbulent heat fluxes with in situ observations over the southeastern Arabian Sea. *Meteorology and atmospheric physics*, *104*(3), 163-175.

Wang, X.; Lee, T.; Mears, C. Evaluation of Blended Wind Products and Their Implications for Offshore Wind Power Estimation. Remote Sens. 2023, 15, 2620. https://doi.org/10.3390/rs15102620

Yu, L., & Weller, R. A. (2008). Objectively analyzed air–sea heat fluxes for the global ice-free oceans (1981–2005). *Bulletin of the American Meteorological Society*, *88*(4), 527-540.